

# Lunar Geochemical Characterisation with Multiwavelength Spectroscopy



A thesis submitted towards partial fulfilment of BS-MS Dual Degree Programme under the

PHYSICS DEPARTMENT

of

INDIAN INSTITUTE OF SCIENCE EDUCATION AND RESEARCH (IISER), PUNE

by:

ABINAYA MARAIVALAVAN

Reg. no. 20171108

under the guidance of

Dr SHYAMA NARENDRANATH

U R RAO SATELLITE CENTRE (URSC), INDIAN SPACE RESEARCH ORGANISATION  
(ISRO), BENGALURU

with the expert member being

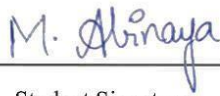
Dr PRASAD SUBRAMANIAN

INDIAN INSTITUTE OF SCIENCE EDUCATION AND RESEARCH (IISER), PUNE

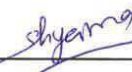


# Certificate

This is to certify that this dissertation entitled “**Lunar Geochemistry and Volatiles**” towards the partial fulfilment of the BS-MS dual degree program at the **Indian Institute of Science Education and Research (IISER), Pune** represents study carried out by **Abinaya Maraivalavan** at **U R Rao Satellite Centre (URSC), Indian Space Research Organisation (ISRO), Bengaluru** under the supervision of **Dr. Shyama Narendranath, Space Astronomy Group, U R Rao Satellite Centre, ISRO, Bengaluru** during the academic year **2023**.



Student Signature



Supervisor Signature

SPACE ASTRONOMY GROUP  
SITE CAMPUS  
ISRO SATELLITE CENTRE  
KARTHIK NAGAR,  
BANGALORE - 560 017



# Declaration

I hereby declare that the matter embodied in the report entitled **Lunar Geochemistry and Volatiles** is the result of the work carried out by me at the **U R Rao Satellite Centre (URSC), Indian Space Research Organisation (ISRO) Bengaluru**, under the supervision of **Dr Shyama Narendranath** and the same has not been submitted elsewhere for any other degree.

M. Abinaya

Student Signature

shyama

Supervisor Signature

SPACE APPLICATIONS  
SITE CAMPUS  
ISRO SATELLITE CENTRE  
KARTHIK ROAD,  
BANGALORE - 560 017



This thesis is dedicated to my mother





# Acknowledgement

I want to start by sincerely thanking my supervisor, Dr K.C. Shyama Narendranath, for her assistance during my master's thesis and for her constant inspiration, motivation, and support. Her guidance was invaluable in my research and writing of this thesis. In addition to my adviser, I would like to express my sincere gratitude to my expert member Dr Parsad Subramanian for his assistance, insightful comments, and suggestions during this project. My sincere gratitude also extends to Nabamita Chaudhuri of Pondicherry University, who provided me with assistance and direction throughout regarding the specifics of ENVI, and IDL. She has been a tremendous morale booster the entire time.

I would like to especially honour my periappa, Dr. T. Chockalingam, for travelling closely with me during this project, engaging in stimulating conversations and mentoring me at every stage of this endeavour and life, in general. I want to express a heartfelt thanks to my family and friends for simply being who they are and supporting me through thick and thin. Finally, and perhaps most importantly, I want to express my deepest gratitude to the Supreme Being for having blessed me with everything and everyone in my life and being my strongest everlasting support.



# Contents

## CHAPTER 1: INTRODUCTION

<b>1.1 THE MOON: EARTH'S ENIGMATIC CELESTIAL NEIGHBOUR.....</b>	<b>3</b>
<b>1.2 LUNAR TERRANES AND GEOLOGY .....</b>	<b>3</b>
<b>1.3 LUNAR FORMATION: MOON'S EVOLUTION .....</b>	<b>4</b>
1.3.1 <i>Surface Composition Today - Key Components.....</i>	5
<b>1.4 Lunar Exploration and Scientific Endeavours.....</b>	<b>5</b>
<b>1.5 Chandrayaan Missions: Unravelling Lunar Mysteries.....</b>	<b>6</b>
1.5.1 <i>Moon Mineralogy Mapper (M3) .....</i>	6
1.5.2 <i>Chandrayaan-2 Large Area X-ray Spectrometer (CLASS) .....</i>	7
1.5.3 <i>Imaging Infra-Red Spectroscopy (IIRS) Instrument.....</i>	9
1.5.4 <i>Comparative Discussion .....</i>	9
<b>1.6 Research Objective and the Region of Interest.....</b>	<b>10</b>
1.6.1 <i>Mare Tranquillitatis: A Fascinating Lunar Maria.....</i>	11
1.6.2 <i>Significance of Mare Tranquillitatis .....</i>	13
<b>1.7 Relevance of Spectral Signatures and Elemental Maps in Mineralogical Studies .....</b>	<b>14</b>
1.7.1 <i>Spectral Signatures and Geological Mapping.....</i>	14
1.7.2 <i>Elemental Maps and Geochemistry.....</i>	15
<b>1.8 Research Scope and Thesis Overview.....</b>	<b>15</b>
<b>2.1 Data Selection and Overlapping .....</b>	<b>17</b>
<b>2.2 M3 .....</b>	<b>20</b>
2.2.1 <i>Data Extraction and Preprocessing .....</i>	20
2.2.2 <i>Integrated Band Depth (IBD).....</i>	22
2.2.3 <i>Spectral Indices .....</i>	22
2.2.4 <i>Modified Gaussian Model (MGM) Method.....</i>	24
2.2.5 <i>Mineral Indices .....</i>	25
<b>2.3 CLASS .....</b>	<b>25</b>
2.3.1 <i>Data Extraction and Preprocessing.....</i>	26
2.3.2 <i>XRF Signals Identification .....</i>	26
2.3.3 <i>Baseline Correction.....</i>	27
2.3.4 <i>Gaussian Peak Fitting .....</i>	28
<b>2.4 IIRS.....</b>	<b>28</b>
2.4.1 <i>Data Extraction and Georeferencing .....</i>	29
2.4.2 <i>Data Preprocessing .....</i>	30
2.4.3 <i>IBD and Spectral Analysis.....</i>	30
<b>3.1 M3 .....</b>	<b>32</b>
3.1.1 <i>Exploration of colour composite of IBD .....</i>	32
3.1.2 <i>Exploration of Colour Composite of the Mineral Indices .....</i>	34
3.1.3 <i>MGM Spectral Studies .....</i>	35
3.1.4 <i>Exploration of Colour Composite of the Spectral Indices .....</i>	37
<b>3.2 IIRS.....</b>	<b>39</b>
3.2.1 <i>Exploration of Colour Composite of IBD .....</i>	40
3.2.2 <i>Spectral Indices Colour Composite Analysis.....</i>	40

<b>3.3 CLASS .....</b>	<b>42</b>
<b>4.1 IBD ANALYSIS BASED ON M3 DATA.....</b>	<b>44</b>
<i>4.1.1 Based on M3 Data.....</i>	44
<i>4.1.2 Based on IIRS Data .....</i>	46
<b>4.2 Modified Gaussian Model (MGM) .....</b>	<b>47</b>
<i>4.2.1 Based on M3 Analysis .....</i>	47
<b>4.3 Mg-Spinel Detection .....</b>	<b>48</b>
<b>4.4 Comparing with CLASS Abundance file.....</b>	<b>49</b>
<i>4.1 Lunar Elemental Analysis Methods .....</i>	49
<i>4.4.2 CLASS Data .....</i>	52
<b>CHAPTER 5: SUMMARY AND CONCLUSION.....</b>	<b>54</b>
<b>REFERENCES.....</b>	<b>57</b>

## ***List of Figures***

<i>Figure 1: Image captured by the Moon Mineralogy Mapper (M3) onboard Chandrayaan 1</i>	<i>7</i>
<i>Figure 2: The Chandrayaan-2 Large Area X-Ray Spectrometer (CLASS)</i>	<i>8</i>
<i>Figure 3: The Imaging Infra-Red Spectroscopy (IIRS) of Chandrayaan-2</i>	<i>10</i>
<i>Figure 4: The Mare Tranquillitatis, a mare region on the near side of the moon</i>	<i>11</i>
<i>Figure 5: Mare Tranquillitatis region recorded by M3 of Chandrayaan-1</i>	<i>12</i>
<i>Figure 6: Geographic locations of elements used to identify a mare region</i>	<i>18</i>
<i>Figure 7: Colour maps of the weight intensities of the elements</i>	<i>18</i>
<i>Figure 8: Lunar surface overlap map of the geometrically corrected data</i>	<i>19</i>
<i>Figure 9: Different stages of preprocessing the reflectance dataset of M3</i>	<i>21</i>
<i>Figure 10: Colour composite generated from IBD parameters of M3G20090202T182612S</i>	<i>33</i>
<i>Figure 11: Mineral indices colour composite generated from M3G20090202T182612</i>	<i>34</i>
<i>Figure 12: Spectra of various pyroxene exposures</i>	<i>36</i>
<i>Figure 13: Spectra of spinel exposures with a strong and broad 2 micron absorption</i>	<i>36</i>
<i>Figure 14: Spectral indices colour composite generated from M3G20090202T182612</i>	<i>38</i>
<i>Figure 15: Modified Gaussian Model applied to Spectra no. 1 and 3</i>	<i>38</i>
<i>Figure 16: Modified Gaussian Model applied to Spectra no. 2, 4 and 5</i>	<i>39</i>
<i>Figure 17: Colour composite generated from ch2_iir_nci_20210621T2245238783_d_img_hw1</i>	<i>41</i>
<i>Figure 18: Colour composite generated from ch2_iir_nci_20210621T2245238783_d_img_hw1</i>	<i>41</i>
<i>Figure 19: The Energy vs Counts/s plot of the combined L1 FITS file of CLASS</i>	<i>42</i>
<i>Figure 20: Gaussian fitted curve for the XRF peaks detected in the combined L1 FITS CLASS files</i>	<i>43</i>

## ***List of Tables***

<i>Table 1: Spectral parameters used to evaluate NIR absorptions</i>	<i>23</i>
<i>Table 2: Band ratio formula and colour assigned for deriving the spectral parameters</i>	<i>25</i>
<i>Table 3: Interpreting the colour composite created from IBD parameters</i>	<i>33</i>
<i>Table 4: Band centres derived from MGM for Spectra no. 1 and 3</i>	<i>37</i>
<i>Table 5: Band centres derived from MGM for Spectra no. 2, 4 and 5</i>	<i>39</i>



## *Abstract*

This study conducts a thorough exploration of the mineralogical composition of a surveyed geochemical anomaly pinpointed within the Mare Tranquillitatis territory of the Moon. Employing a multidisciplinary methodology, it harnesses data from the Moon Mineralogy Mapper (M3) on Chandrayaan-1, the Imaging Infra-Red Spectrometer (IIRS), and Chandrayaan 2's Low Area Soft X-Ray Spectrometer (CLASS) onboard Chandrayaan-2. The principal aim of this research is to unravel the intricate mineralogical tapestry underlying this lunar anomaly. To achieve this, colour composite images were meticulously crafted utilising integrated band depth parameters and mineral indices, serving as a visual representation of the mineralogical variations within the study area. Subsequently, the unique spectral signatures corresponding to these composite colours, as discerned from the M3 dataset, were scrutinised in detail. Furthermore, the Modified Gaussian Model (MGM) deconvolution technique was applied to these spectra, enhancing the precision of mineral identification. A parallel methodology was implemented to analyse the IIRS dataset, culminating in a correlation with an abundance file derived from the CLASS data. The outcomes of this extensive spectral analysis unveil a landscape characterised by heterogeneous lithologies. Predominantly, the study region comprises anorthosite, complemented by the presence of pyroxene-bearing and olivine-bearing basaltic lithologies. Notably, significant topographic disparities are observed between the eastern and western regions of the Mare Tranquillitatis. These differences manifest not only in topography but also in the spatial dispersal of spectral units and compositional trends. The western Mare area exhibits a higher prevalence of olivine-bearing material within the olivine-pyroxene mixture, while the eastern Mare prominently exhibits pyroxene-bearing material. The correlation of spectral findings with lunar morphology yields intriguing insights. Pyroxene-rich compositions are notably associated with fresh craters and their ejecta, indicative of their geological origins. In contrast, olivine is found to be pervasive across the lunar surface, dispersed widely, and often distributed along the ejecta blankets of large impact craters. This association suggests that the pyroxene-hosted layer likely resides beneath the olivine-bearing layer. The noticed mineral assemblages are hypothesized to have arisen through physical blending processes during the impact cratering episodes that have shaped the lunar landscape.





---

## CHAPTER 1: INTRODUCTION

---

### 1.1 THE MOON: EARTH'S ENIGMATIC CELESTIAL NEIGHBOUR

The Moon is one of the most prominent and easily observable celestial objects in the night sky. Its regular and predictable appearance made it a natural focus of attention for early civilizations. Throughout history, various civilizations have pondered its enigmatic surface, leading to the early classification of the lunar terrain into two distinct regions: Terra and Maria terranes. The 17th century marked the formal division of the lunar surface into these terranes, with the Terra thought to represent the continent and the Maria the oceanic region<sup>[1]</sup>. As technology advanced, the Moon became an even more attractive target for study. The space race during the Cold War era led to the first human landing on the Moon in 1969 as part of NASA's Apollo 11 mission. This event marked a major milestone in human history and further fuelled interest in lunar exploration. The above-mentioned classification was recognized to be inaccurate, with the increase in scientific understanding, and the true nature of these lunar terranes began to emerge.

### 1.2 LUNAR TERRANES AND GEOLOGY

The Maria terrane, characterised by its dark appearance, was found to be the result of ancient volcanic activity, formed by vast lava plains that flooded low-lying areas. As such, it is relatively younger than the Terra terrane and exhibits lower elevation levels. Conversely, the Terra terrane, representing the lighter areas of the Moon, is older and more elevated, boasting a greater number of impact craters accumulated over an aeon.

In the pursuit of a deeper comprehension of the lunar landscape, researchers turned to geochemistry and elemental abundances to delineate the different lunar terranes more accurately. Their investigations revealed three distinct terranes on the Moon's surface:

1. The Procellarum KREEP Terrane (PKT): The nearside Procellarum KREEP Terrane (PKT) is distinguished by its enrichment in potassium (K), rare earth elements (REE), and phosphorus (P)<sup>[2]</sup>, setting it apart from other lunar regions<sup>[3]</sup>.

2. The Feldspathic Highland Terrane (FHT): The far side Feldspathic Highland Terrane (FHT) is predominantly composed of ancient anorthositic materials with low levels (4.2-5.5 wt%) of iron oxide, FeO, and enriched in thorium (Th). The FHT on the far side of the Moon stands as one of the oldest and most pristine rock types known to us [4].
3. The South Pole-Aitken Basin Terrane: The South Pole-Aitken Basin Terrane, closely related to the Feldspathic Highlands Terrane, represents deep crustal materials with thorium levels lying between those of the PKT and FHT [5]. The terrane has its emergence in a large impact that transpired early in the Moon's history and which had a crucial impact on the Moon's thermal evolution[3].

Each of these terranes has a distinct geological history, elemental composition, and thermal evolution, adding to the Moon's diverse and intricate geology [6][7].

### **1.3 LUNAR FORMATION: MOON'S EVOLUTION**

As Earth's closest celestial neighbour, the lunar surface has long captivated the imagination of astronomers, scientists, and explorers alike. Its desolate beauty and enigmatic history make it a crucial object of study in planetary science. This introduction sets the stage by highlighting the importance of lunar surface composition, delving into the Moon's evolution, outlining the key components of its surface today, and establishing the motivation for this work, particularly the study of water adsorption and its dependence on surface geochemistry.

The Moon's composition holds essential clues about its formation and origin. The Giant Impact Hypothesis, the leading theory, posits that a Mars-sized object collided with the young Earth, leading to the formation of the Moon [8]. The composition of lunar rocks and minerals provides insights into the validity of this theory and helps unravel the Moon's evolutionary history. Understanding such lunar surface composition aids in comprehending differentiation processes within the Moon. These processes include the separation of distinct layers, such as the crust, mantle, and potentially a small core. Analysing the composition of these layers sheds light on the Moon's early thermal history [9].

### *1.3.1 Surface Composition Today - Key Components*

Comprehending the Moon's composition and evolution requires an exploration of its differentiation techniques. Initially in its history, the Moon experienced differentiation, separating into distinct layers, including the crust, mantle, and probably a trivial metallic core <sup>[10]</sup>. The configuration of these layers and the timing of differentiation events can provide insights into the Moon's formation and its relationship with the Earth <sup>[11]</sup>.

1. **Regolith:** The lunar regolith, a deposit of loose, fragmented material casing the solid bedrock, is an intricate mixture of small rock besides mineral fragments. By studying the composition of the regolith, we can glean insights into the Moon's geological history, including the intensity and frequency of impact events that have shaped its surface.
2. **Rocks and Minerals:** The Moon's surface is adorned with an array of rocks and minerals. These include basalts, which are rich in iron and magnesium, anorthosites composed of the mineral anorthite, and various breccias formed by impacts. Each rock type offers a unique piece of the lunar puzzle, helping us piece together its geological past.
3. **Volatiles:** The occurrence of volatiles on the Moon's surface has been a recent revelation. Water ice, in particular, has been detected in eternally shadowed sections near the lunar poles. Studying the distribution and characteristics of these volatiles not only provides valuable scientific insights but also has profound implications for future lunar exploration and colonisation.

## **1.4 Lunar Exploration and Scientific Endeavours**

To make a much more significant classification of the Moon and unravel its many mysteries, space agencies worldwide are endeavouring to explore the lunar surface further. Through robotic missions, remote sensing, and future crewed missions, scientists and researchers hope to grow a deeper perspective of the Moon's geology, history, and potential resources. These explorations not only enhance our knowledge of the Moon but also provide valuable insights into the primary history of our solar system and the broader field of planetary science. One such attempt by the Indian Space Research Organisation (ISRO) made significant contributions to this endeavour with its Chandrayaan missions. Launched in 2008,

Chandrayaan-1 <sup>[12]</sup> marked India's entry into lunar exploration and played a pivotal role in expanding our understanding of the lunar surface.

### **1.5 Chandrayaan Missions: Unravelling Lunar Mysteries**

Chandrayaan-1 was equipped with sophisticated scientific instruments, including the Moon Mineralogy Mapper (M3), an international payload with a wavelength range of 0.4-3 micron. M3's capabilities allowed it to identify crucial features on the lunar surface, such as water absorption structures, Mg-Spinel, and increased sodium content. Notably, M3 made groundbreaking discoveries, revealing the existence of hydroxyl and water-ice molecules in high-latitude lunar regions <sup>[13]</sup> <sup>[14]</sup>.

Building on the triumph of Chandrayaan-1, ISRO launched Chandrayaan-2 <sup>[15]</sup> in 2019, aiming to deepen our understanding of the Moon's mineralogy, topography, elemental abundance, and exosphere. One of Chandrayaan-2's primary objectives was to investigate the signatures of hydroxyl and water ice on the lunar surface. To achieve this, the mission carried a suite of advanced scientific payloads, each designed to provide crucial insights into lunar geology. Among those, the Imaging Infra-Red Spectrometer (IIRS) and the Chandrayaan-2 Large Area X-Ray Spectrometer (CLASS) have been the payloads of interest for this project<sup>[16]</sup>.

#### *1.5.1 Moon Mineralogy Mapper (M3)*

The Moon Mineralogy Mapper (M3) is a scientific instrument aboard Chandrayaan-1, India's lunar orbiter. M3 is designed to report the mineralogical structure of the lunar surface by analysing the sunlight reflected from the Moon across a wide range of wavelengths in the near-infrared and short-wavelength infrared regions <sup>[17]</sup>. Figure 1 displays the image of the lunar surface<sup>[85]</sup> as apprehended by M3.

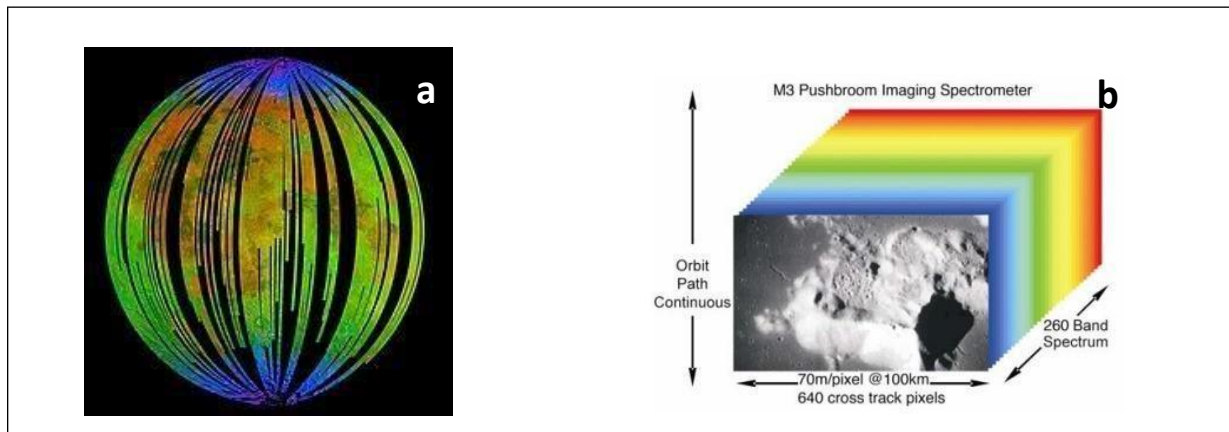


Figure 1: Image captured by the Moon Mineralogy Mapper (M3) onboard Chandrayaan 1. (a) Moon mosaic created with Moon Mineralogy Mapper photos. Water's sign is depicted in blue, surface brightness is indicated in green through gauging reflected infrared radiation from the sun, and an iron-containing mineral known as pyroxene is shown in red. (b) *The M3 pushbroom instrument concept: Two dimensions of geographic information and one dimension of spectral characteristics are combined to create an image cube of data.*

The working principle of M3 is based on the technique of reflectance spectroscopy. When sunlight illuminates the lunar surface, the minerals present in the surface material absorb certain wavelengths of light while reflecting others. Each mineral has its unique spectral signature, which is characterised by specific absorption characters or "bands" in the reflectance spectra. These absorption characters are related to the molecular vibrations of the mineral's crystal lattice structure, which interact with incoming light at specific wavelengths [18] [19].

M3 uses a spectrometer to split the incoming sunlight into its constituent wavelengths. The spectrometer measures the amount of light reflected by the lunar surface at different wavelengths, creating a reflectance spectrum. By analysing the reflectance spectrum and the spectral signatures, M3 can identify and map various minerals on the lunar surface, including those connected with water and hydroxyl molecules [13] [20].

### 1.5.2 Chandrayaan-2 Large Area X-ray Spectrometer (CLASS)

The Chandrayaan-2 Large Area X-ray Spectrometer (CLASS) is a scientific instrument onboard India's lunar orbiter, Chandrayaan-2. CLASS is designed to study the elemental composition of the lunar surface using X-ray fluorescence spectroscopy.

The working principle of CLASS is grounded on the interaction of X-rays with the lunar surface material. When X-rays with sufficient energy strike the lunar surface, they can ionize

inner-shell electrons of atoms in the surface material. This ionisation process results in the emission of characteristic X-rays from the atoms. The energy of these emitted X-rays is specific to the elemental composition of the material [21].

CLASS consists of a collimator and a detector. The collimator is used to focus the incoming X-rays onto a specific region of the lunar surface, while the detector measures the energy and intensity of the characteristic X-rays discharged from the surface material (as shown in Figure 2).

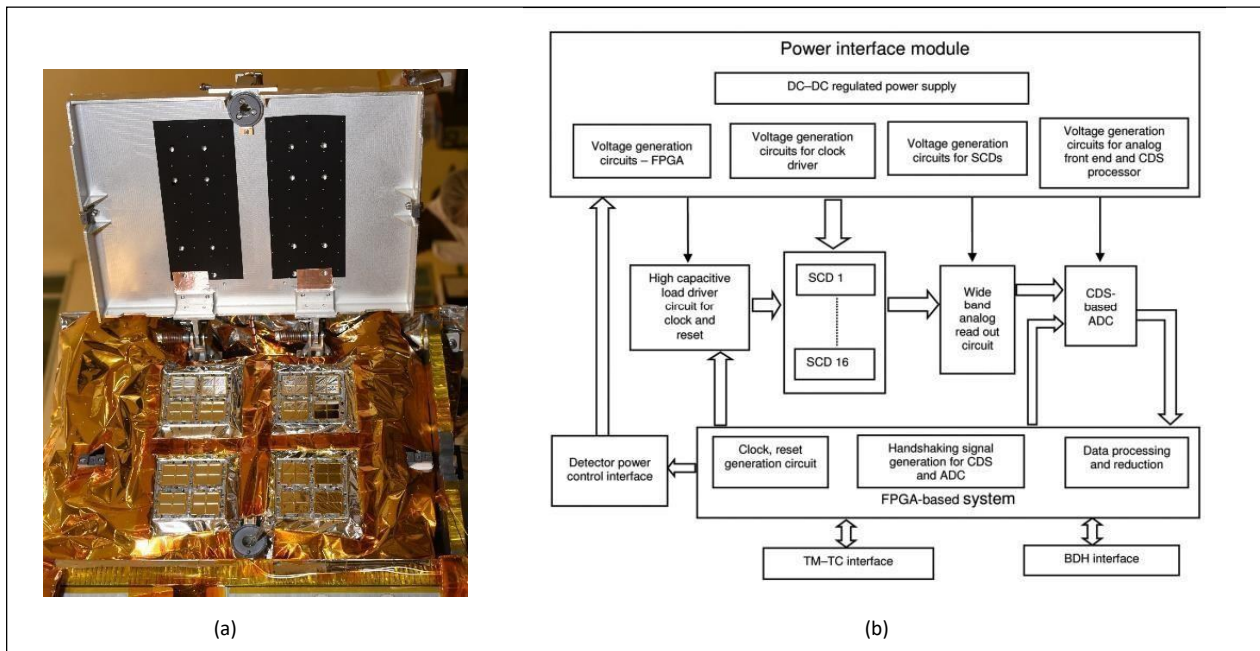


Figure 2: The Chandrayaan-2 Large Area X-Ray Spectrometer (CLASS); (a) CLASS Flight instrument. (b) Block diagram of the electronics of the CLASS instrument.

The instrument is capable of detecting X-rays in the energy range of 1 to 20 kiloelectron<sup>[16]</sup> volts (keV). Different elements have their unique characteristic X-ray energies, allowing CLASS to identify and quantify the abundance of various elements present on the lunar surface [22]. By scanning the lunar surface and measuring the X-ray fluorescence signals at different locations, CLASS can create elemental maps of the Moon. These maps provide valuable information about the distribution of elements such as silicon, aluminium, calcium, iron, and titanium, among others.

### *1.5.3 Imaging Infra-Red Spectroscopy (IIRS) Instrument*

Another key instrument onboard Chandrayaan-2 was the Imaging Infra-Red Spectroscopy (IIRS) instrument, which significantly extended the wavelength range compared to M3, covering up to 5 micron. IIRS played a vital role in mapping the lunar surface and studying minerals, water molecules, and hydroxyl presence in greater detail. Its findings complemented and validated the discoveries made by M3, providing unambiguous detections of OH, H<sub>2</sub>O, and water-ice signals on the Moon <sup>[23]</sup>.

The working principle of IIRS is built on the interaction of infrared radiation with the lunar surface material. Infrared radiation lies in the electromagnetic spectrum between visible light and radio waves, with longer wavelengths than visible light. When infrared radiation is directed towards the lunar surface, it interacts with the mineral crystals and molecules present in the regolith (the layer of loose soil and rocks on the lunar surface).

Different minerals and materials have their unique spectral signatures in the infrared range. These spectral signatures manifest as specific patterns of absorption and reflection of infrared light at various wavelengths. The positions and shapes of these absorption and reflection features reveal the mineralogical configuration of the surface material. It is by analysing these absorption features, that IIRS identified and mapped the occurrence of hydroxyl and water molecules on the Moon, providing crucial insights into lunar water resources <sup>[24]</sup>.

IIRS is equipped with a spectrometer that measures the intensity of infrared radiation reflected or emitted from the lunar surface at various wavelengths. The spectrometer divides the incoming infrared radiation into different wavelength bands and records the energy at each wavelength. The resulting data forms a spectral signature, often referred to as an infrared spectrum, which provides information about the minerals and compounds present in the lunar soil.

### *1.5.4 Comparative Discussion*

M3 and IIRS complement each other by providing both mineral composition data (M3) and thermal information (IIRS) about the same lunar areas. This synergy enhances the overall understanding of the Moon's surface properties. CLASS complements M3 and IIRS by focusing on the elemental composition, which is a key aspect of lunar geology. It provides

data on the presence and abundance of specific elements, giving insights into the Moon's history and formation.

In summary, these three instruments on the Chandrayaan spacecrafts serve different but complementary purposes. M3 specialises in mineral identification, IIRS focuses on thermal properties and mineral mapping, and CLASS provides elemental composition data. Together, they provide a comprehensive view of the Moon's surface, aiding in the understanding of lunar geology, composition, and its history.

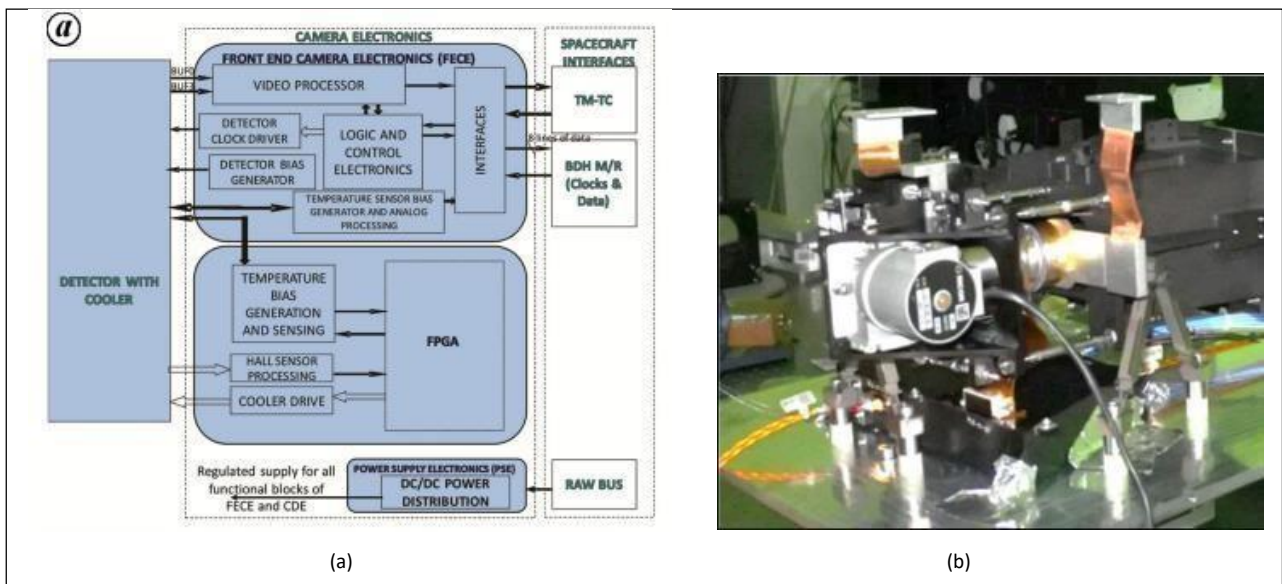


Figure 3: The Imaging Infra-Red Spectroscopy (IIRS) of Chandrayaan-2; (a) Electronic block diagram of the payload. (b) IIRS focal plane assembly.

### 1.6 Research Objective and the Region of Interest

This research project endeavours to effectively delve into a particular Mare region on the surface of the Moon. For this, we require a combination of critical datasets from multiple instruments. Hence, the chosen area must be covered by the essential hyperspectral imaging payloads, including M3, IIRS, and the X-ray spectrometer (CLASS). These advanced instruments have played pivotal roles in unravelling the lunar surface's mysteries, providing invaluable insights into the Moon's composition and thermal characteristics. This led to the choice of the Mare Tranquillitatis region as the region of interest.

By concentrating our research efforts on the intersecting region that falls under the purview of M3, IIRS, and CLASS, we aim to harness the full potential of their diverse capabilities.



The combined data from these instruments will enable us to conduct a comprehensive correlation study between water retention and geochemistry, shedding light on the intricate interplay of these factors within the Mare Tranquillitatis region.

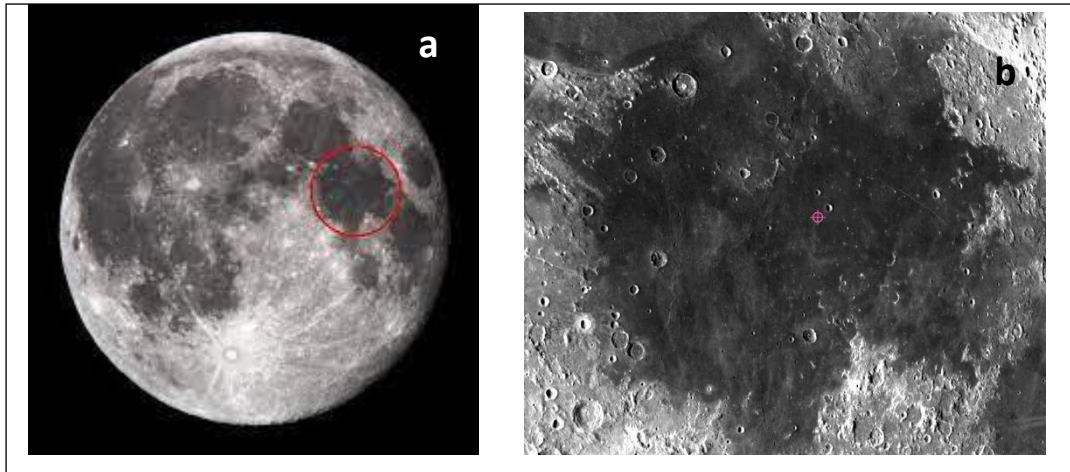


Figure 4: The Mare Tranquillitatis, a mare region on the near side of the moon. (a) Location of Mare Tranquillitatis on the Moon, (b) Zoomed-in image of the Mare Tranquillitatis region taken from LROC quick maps

### 1.6.1 Mare Tranquillitatis: A Fascinating Lunar Maria

Mare Tranquillitatis, which translates to the "Sea of Tranquillity", is one of the most prominent lunar maria on the near side of the Moon (shown in Figure 4). Located at approximately  $8.5^{\circ}\text{N}$  latitude and  $31.4^{\circ}\text{E}$  longitude, this expansive region covers an area of approximately 87,000 square kilometres <sup>[25]</sup>. It is a basaltic plain, formed by ancient volcanic activity that occurred billions of years ago <sup>[26]</sup>. Figure 5 shows a 2-D map of the lunar surface highlighting the Mare Tranquillitatis region.

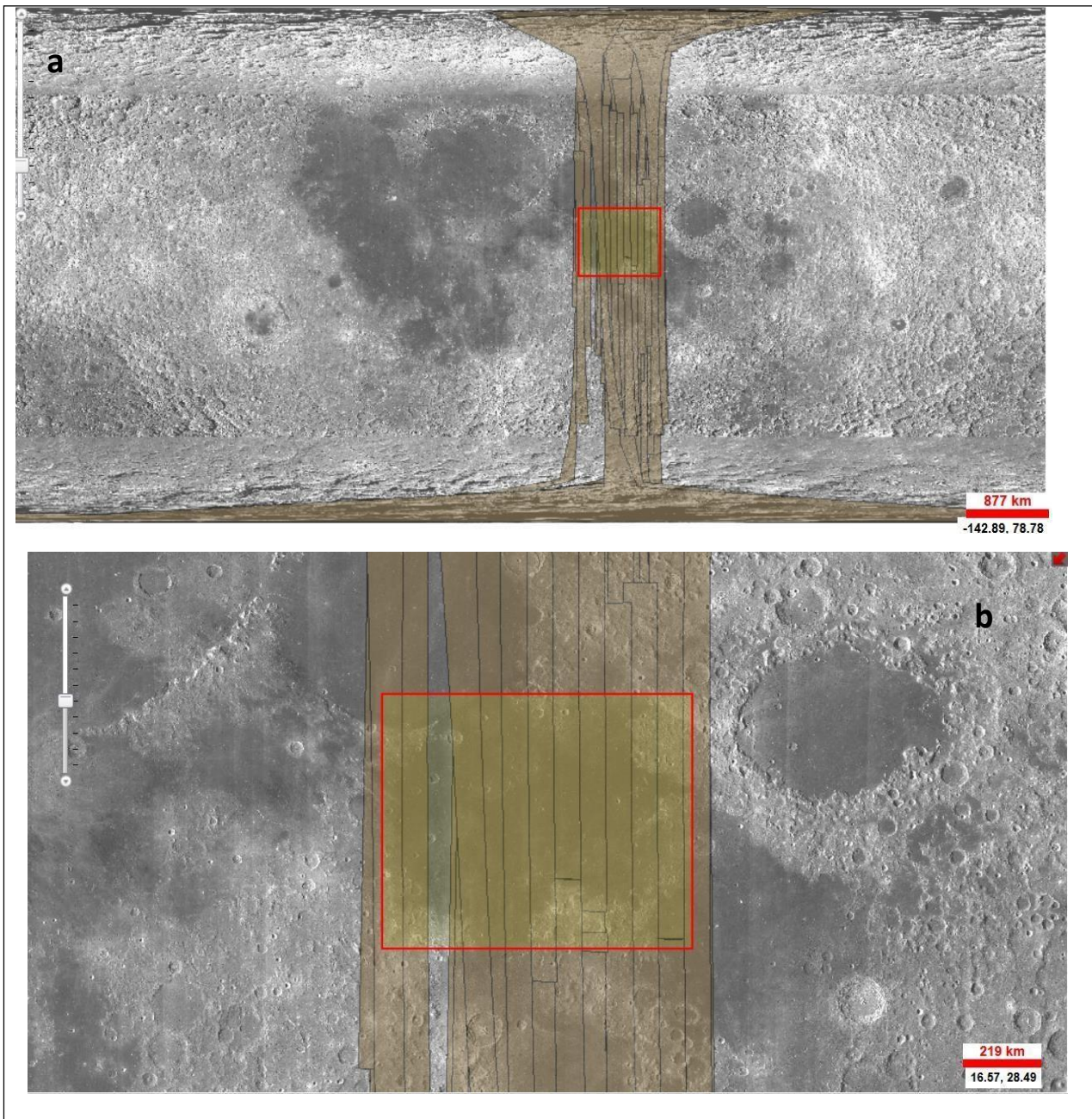


Figure 5: Mare Tranquillitatis region recorded by M3 of Chandrayaan-1; (a) Lunar map with the scale on the bottom right of the image. The shaded region is where M3 has recorded its data in the global mode with the region marked in red, being the required area of interest. (b) Zoomed in to the area of interest.

The Mare Tranquillitatis is primarily composed of basaltic lava flows that originated from volcanic eruptions during the Moon's early history. These eruptions released vast quantities of magma onto the lunar surface, filling low-lying impact basins and creating the smooth, dark plains characteristic of lunar maria. The volcanic activity that formed Mare Tranquillitatis occurred around 3.8 to 3.5 billion years ago, making it one of the relatively younger lunar features <sup>[27]</sup>.

Mare Tranquillitatis is surrounded by the lunar highlands, which are comprised of ancient anorthositic materials. These anorthosites are supposed to have formed from the solidification of the early lunar magma ocean and are characterised by their light-coloured appearance <sup>[28]</sup>. The transition between the lunar highlands and the mare regions, like Mare Tranquillitatis, is often marked by a sharp boundary known as the "rille," which separates the mare-fill material from the ancient highland rocks.

Despite the extensive volcanic resurfacing, Mare Tranquillitatis still preserves a record of its early history through numerous impact craters that dot its surface. The size and density of these impact craters provide important clues about the region's geological evolution and the intensity of impacts during different epochs of lunar history<sup>[27]</sup>. The presence of such impact features also suggests that Mare Tranquillitatis has remained relatively undisturbed by volcanic activity for billions of years.

#### *1.6.2 Significance of Mare Tranquillitatis*

The Mare Tranquillitatis region exhibits interesting compositional variations compared to other lunar maria. Remote sensing data from lunar missions, including Chandrayaan-1 and Chandrayaan-2, have revealed that this region contains higher concentrations of aluminium (Al) and silicon (Si) relative to the lunar basalts found in other maria <sup>[29]</sup>. These compositional variations make the Mare Tranquillitatis an intriguing location for studying lunar geochemistry and understanding the origin and evolution of mare basalts.

The mare basalts in this region are relatively young, with radiometric dating suggesting they formed between 3.5 to 3.8 billion years ago, making them some of the youngest volcanic deposits on the Moon <sup>[26]</sup>. The basalts are composed of dark, iron-rich volcanic rocks, primarily basaltic lava flows, which give the maria their characteristic dark appearance and low albedo (reflectivity). These lava flows were extruded onto the lunar surface through volcanic eruptions, spreading out to form extensive plains that we observe today <sup>[24]</sup>.

Moreover, the availability of data from the Chandrayaan-1 and Chandrayaan-2 missions makes the Mare Tranquillitatis region an ideal target for studying water retention and its correlation with geochemistry. The M3 and IIRS on Chandrayaan-2 have provided valuable information about the presence of hydroxyl and water-ice molecules in high-latitude lunar regions <sup>[13][23]</sup>. Additionally, CLASS has offered insights into the elemental composition of

the lunar surface <sup>[22]</sup>. The combination of these data sources allows for a comprehensive investigation of the possible links between water retention and geochemistry within the Mare Tranquillitatis region.

The study of water retention and geochemistry in this region is of significant importance for advancing lunar science and exploring potential water resources on the Moon. Understanding the distribution and abundance of water and its relation to the geological composition can have implications for future lunar missions, resource utilisation, and the sustainability of human presence on the Moon.

### **1.7 Relevance of Spectral Signatures and Elemental Maps in Mineralogical Studies**

While the Mare Tranquillitatis region is not one of the areas typically associated with the presence of water ice, the knowledge gained from studying its geological and mineralogical characteristics can contribute to our understanding of lunar water resources. By investigating the region's geological history and chemical composition, scientists can infer potential sources of water and hydroxyl molecules on the Moon and explore their relation to the lunar volcanic processes that formed the mare basalts <sup>[30]</sup>.

The Mare Tranquillitatis region has been subject to extensive spectroscopic studies using instruments like the M3 and the IIRS instrument. The spectroscopic analysis involves measuring the reflected sunlight from the lunar surface across various wavelengths, capturing the unique spectral signatures of different minerals and molecules present on the Moon <sup>[30]</sup>. By analysing these spectral signatures, researchers can identify the mineral composition of the mare basalt and other geological features within the Mare Tranquillitatis region.

#### *1.7.1 Spectral Signatures and Geological Mapping*

Spectral signatures and geological mapping are essential tools used by lunar scientists to study the mineralogical composition and distribution of materials on the Moon's surface. Spectral signatures are unique reflectance patterns exhibited by minerals at specific wavelengths, allowing the identification of mineral species based on their characteristic absorption features. Wavelength position of absorption, band depth maps, and elemental maps obtained from these instruments provide crucial information for mineralogical studies.

The Mare Tranquillitatis region has been subject to extensive spectroscopic studies using instruments like the M3 and the IIRS instrument. The spectroscopic analyses measure the reflected sunlight from the lunar surface across various wavelengths, capturing the unique spectral signatures of different minerals and molecules on the Moon <sup>[22]</sup>. By analysing these spectral signatures, one can identify the mineral composition of the mare basalt and other geological features within the Mare Tranquillitatis region.

### *1.7.2 Elemental Maps and Geochemistry*

Spectral analysis allows for the identification of characteristic absorption features in the reflected light spectra, which are indicative of specific minerals or molecules. The presence of hydroxyl and water molecules on the lunar surface is often identified by their distinct absorption features in the near-infrared region of the spectrum. Band depth maps provide spatial information about the abundance and distribution of these features across the lunar surface, including the Mare Tranquillitatis region. The analysis of such maps helps understand the potential presence and distribution of water-ice<sup>[85]</sup> and hydroxyl molecules in the lunar regolith <sup>[31]</sup>.

In addition to spectroscopic analyses, CLASS provides elemental maps of the lunar surface. By detecting X-rays emitted by the lunar regolith when bombarded by solar X-rays, CLASS can determine the abundance of various elements present on the Moon <sup>[32]</sup>. These elemental maps offer insights into the geochemistry of the Mare Tranquillitatis region, helping researchers understand the distribution of key elements like aluminium (Al), silicon (Si), iron (Fe), and others, which play a crucial role in lunar geological processes <sup>[30]</sup>.

The combination of spectral signatures, band depth maps, and elemental maps from advanced lunar instruments offers a comprehensive understanding of the geological history, mineralogical composition, and potential resources of the Mare Tranquillitatis region. This wealth of information serves as a cornerstone for scientific investigations and has significant implications for future lunar exploration endeavours.

## **1.8 Research Scope and Thesis Overview**

As we embark on this exploration of the lunar landscape, guided by the latest advancements in technology and our unwavering passion for scientific discovery, we anticipate uncovering

novel insights into the Mare Tranquillitatis's unique geological history and mineralogical characteristics. By correlating data from M3, IIRS, and CLASS, we aim to shed light on the relationship between water retention and geochemistry in this intriguing lunar region. The comprehensive analysis of spectral signatures, wavelength positions of absorption features, band depth maps, and elemental maps will enhance our understanding of lunar water resources, geology, and potential implications for future lunar missions and human exploration.

The combination of M3, IIRS, and CLASS data offers a multi-faceted view of the Moon's mineralogical and chemical makeup. By studying different regions' mineral and elemental composition, scientists can unravel the Moon's geological history and processes, including volcanic activity, impact events, and the formation of different lunar terranes <sup>[33]</sup>.

Through this research, we aspire to contribute to the ever-expanding frontier of lunar knowledge, further cementing the Moon's position as a compelling frontier for scientific exploration and human curiosity. Python is the programming language being used to write all of the computational work while delving into the data acquired from Chandrayaan payloads. In addition to that, applications like ENVI, QGIS, and XSPEC have also been used at various stages of the project.

---

## CHAPTER 2: DATA AND METHODOLOGY

---

### 2.1 Data Selection and Overlapping

The lunar maria are vast, dark basaltic plains that were created on the Moon by ancient asteroid impacts on the far side of the body that sparked volcanic activity on the other (near) side. They appear darker to the human eye because of their composition, which is iron-rich<sup>[34]</sup> and makes them less reflective than the "highlands". About 16% of the lunar surface is covered by maria<sup>[35]</sup>, especially on the side that is visible from Earth. Iron, titanium, and other elements are more prevalent in the maria's basalts than in the highlands. For instance, while most terrestrial basalts<sup>[86]</sup> have TiO<sub>2</sub> abundances<sup>[36]</sup> significantly lower than 4 wt.%, TiO<sub>2</sub> abundances in mare basalts can reach up to 15 wt.%.

The volcanic rocks that make up the lunar maria, called lunar mare basalts, frequently contain aluminium. Aluminium is commonly present in these basalts at higher amounts than other elements. Two minerals that are typically found in these basalts that contain aluminium are pyroxenes and plagioclase feldspar<sup>[37]</sup>. In contrast to elements like iron (Fe) and titanium (Ti), however, the aluminium content of lunar mare basalts is not exceptionally high<sup>[38]</sup>. The elemental abundances may vary depending on the exact position and geological context inside the mare, however, based on the weight percentages, it is possible to classify whether a certain region of the Moon is a mare region or not. The mare basalts include a greater amount of iron, titanium, and generally a marginally lower abundance of aluminium.

The abundance file on PRADAN is a CSV file that includes the geographic latitude and longitude positions of each point recorded along with the elemental weight percentages recorded. It is based on the data collected by the CLASS instrument on Chandrayaan-2. Since the project's main objective was to investigate a mare region on the near side of the lunar surface, the data points from the mare region had to be extracted. Figure 6 below contains the geographical location where CLASS has recorded the Ti, Fe and Al weight percentages. Figure 7 shows the weight intensity of the respective elements in the selected region of interest.

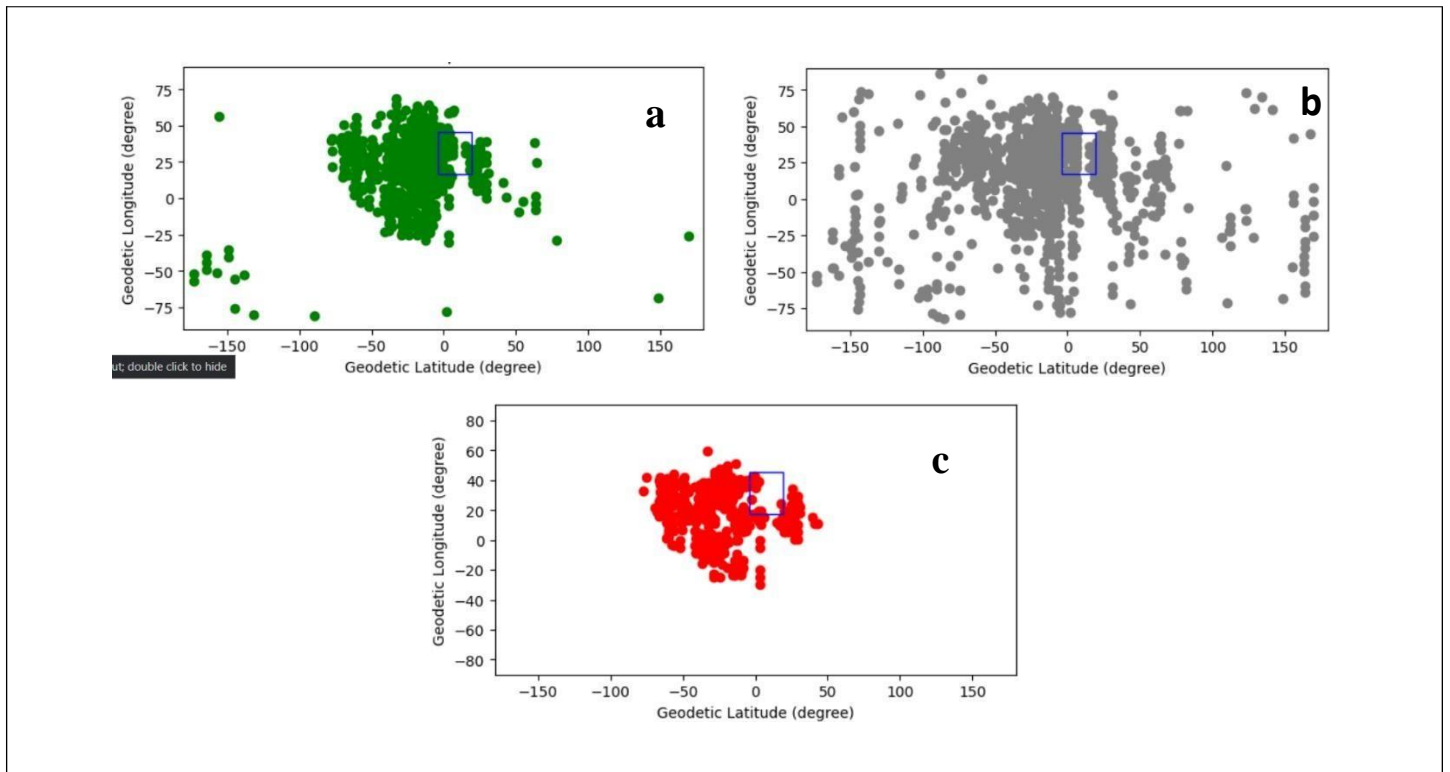


Figure 6: Plot marking the positions of geographic locations on the lunar surface containing the elements used to identify a mare region based on the elemental abundance recorded by CLASS. The blue grid in the plots represents the region of interest (Mare Tranquillitatis) selected for this study. (a) Geographic locations containing Aluminium (b) Geographic locations containing Iron and (c) Geographic locations containing Titanium

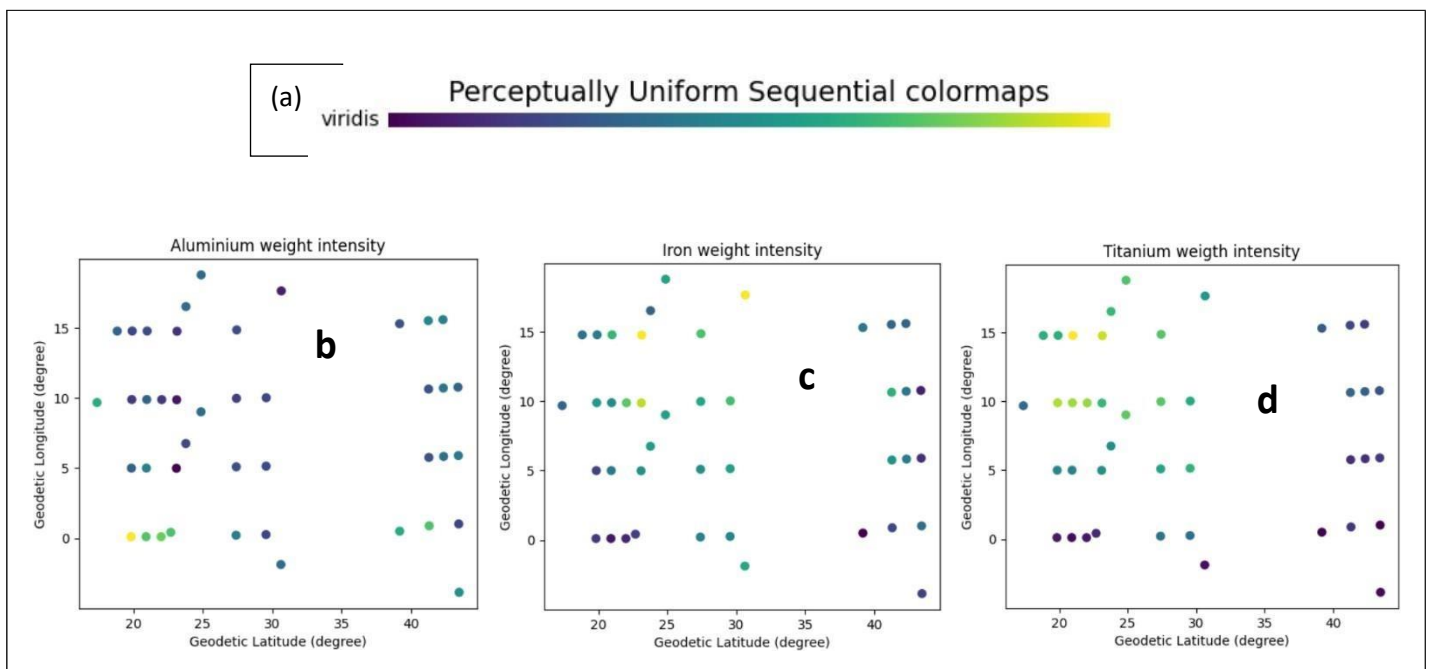


Figure 7: Colour maps of the weight intensities of the elements shown in Figure 6. These colour maps help to identify the mare regions of the lunar surface based on the element abundance of CLASS. (a) Index of the colour map. (b) Weight intensity of Aluminium. (c) Weight intensity of Iron. (d) Weight intensity of Titanium.



Choosing an area that has been recorded by all the 3 instruments will provide an opportunity to understand the region better. To have such a comparative study, it was necessary to choose a region that has been recorded by M3, CLASS and IIRS. Now that the mare region data recorded by CLASS has been segregated out, the respective shapefiles based on data from CLASS and IIRS were downloaded from the other downloads section of the Policy based data Retrieval, Analytics, Dissemination And Notification system, PRADAN (<https://pradan.issdc.gov.in/ch2/>) a web application developed by Indian Space Science Data Centre, ISSDC. The shapefiles from CLASS and IIRS required geometric correction to treat the invalid or error-containing data points, for which the QGIS software <sup>[39]</sup> (<https://www.qgis.org/en/site/>) came in handy. After individually correcting the invalid and error data points in both the shapefiles, the valid and the corrected data were merged into one single file post and these merged files were overlapped to receive the geometrical coordinates of the common area of observance, as shown in figure 8. The M3 datasets were further downloaded in this area of overlap of CLASS and IIRS. The datasets recorded by M3 were available for download from Lunar Orbital Data Explorer, ODE (<https://ode.rsl.wustl.edu/moon/productsearch>) from NASA's Planetary Data System (PDS) Geosciences Node. This final overlap led to the choice of Mare Tranquillitatis as the region of interest for this study.

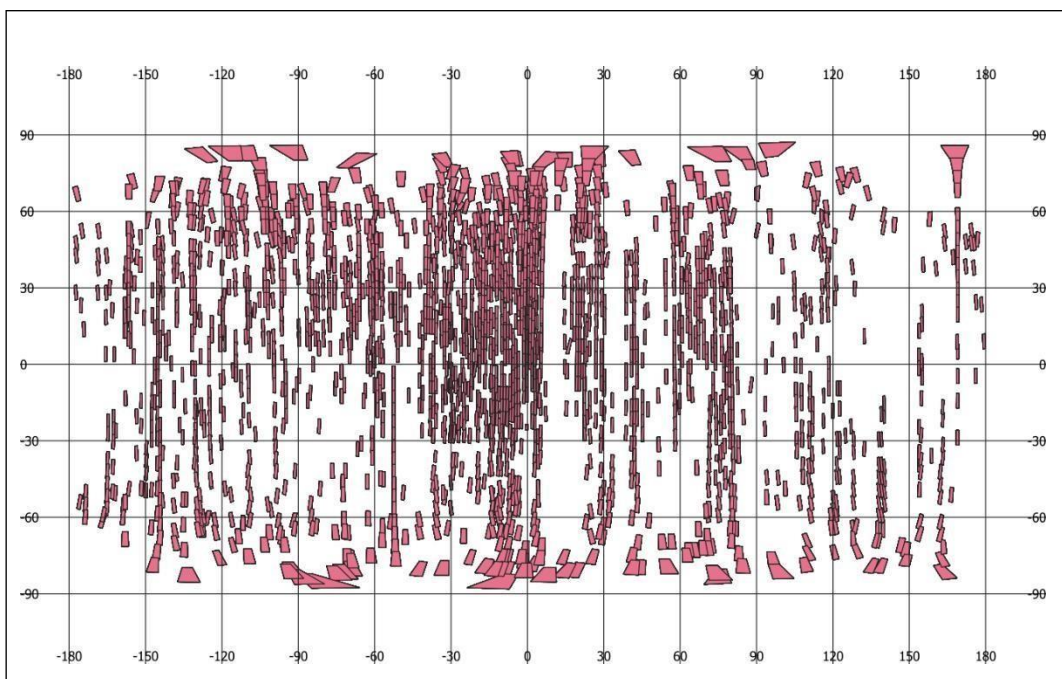


Figure 8: Lunar surface overlap map of the geometrically corrected data of CLASS and IIRS using QGIS. Geographic 2D CRS: EPSG:4326 WGS 84

## 2.2 M3

### 2.2.1 Data Extraction and Preprocessing

M3, a visible-near infrared imaging spectrometer covering the spectral range of 0.4 to 3 micron, was part of the Chandrayaan-1 mission by the Indian Space Research Organisation (ISRO)<sup>[12]</sup>. During the OP2A optical period, it collected reflectance (I/F) data. We obtained two datasets, M3G20090202T142951 and M3G20090202T182612, from the Lunar Orbital Data Explorer website. These datasets were collected in global mode with a spatial resolution of 280 meters per pixel. We used the corresponding LOC file to georeference the M3 data, and a spatial subset was applied to focus on the zone of curiosity. Beyond 2.5-micron, spectral bands potentially were affected by thermal emission, were excluded from our analysis. We refrained from creating a mosaic due to the lack of geographical overlap between the two images. Each image underwent individual processing using ENVI software. To boost the data by reducing noise, both forward and reverse Minimum Noise Fraction (MNF) techniques<sup>[40][41]</sup> were applied. Additionally, shadow masking was employed to eliminate pixels in shadowed regions for further processing. (Figure 9)

For studying the mineral composition of the area of interest, we performed image analysis by computing spectral parameters, including Integrated Band Depth (IBD)<sup>[40][42][43]</sup> and spectral indices (ratios)<sup>[44]</sup>, using the calibrated M3 data<sup>[40][42][43]</sup>. Both serve as methods for characterizing the mineral configuration of the region. IBD focuses on distinguishing the band depth around any absorption feature noted, while mineral indices involve the ratio of reflectance maxima to reflectance minima for the minerals that are under examination<sup>[40]</sup>. Since both the methods target the same lunar materials, consistent outcomes were awaited. Colour composites were then generated using these spectral parameters, highlighting disparities in mineral configuration<sup>[40]</sup>. Spectral signatures were extracted from the noise-reduced M3 data for each unique colour representation observed in the created colour composite depiction<sup>[40]</sup>.

The spectra of the reflective portion of the sun spectrum are provided by the hyperspectral images captured by M3, which also enables us to employ methods like spectral mixture analysis to decode the mixed spectral information and create abundance maps of surface features on the moon. The general concave form of a spectrum should be eliminated to allow

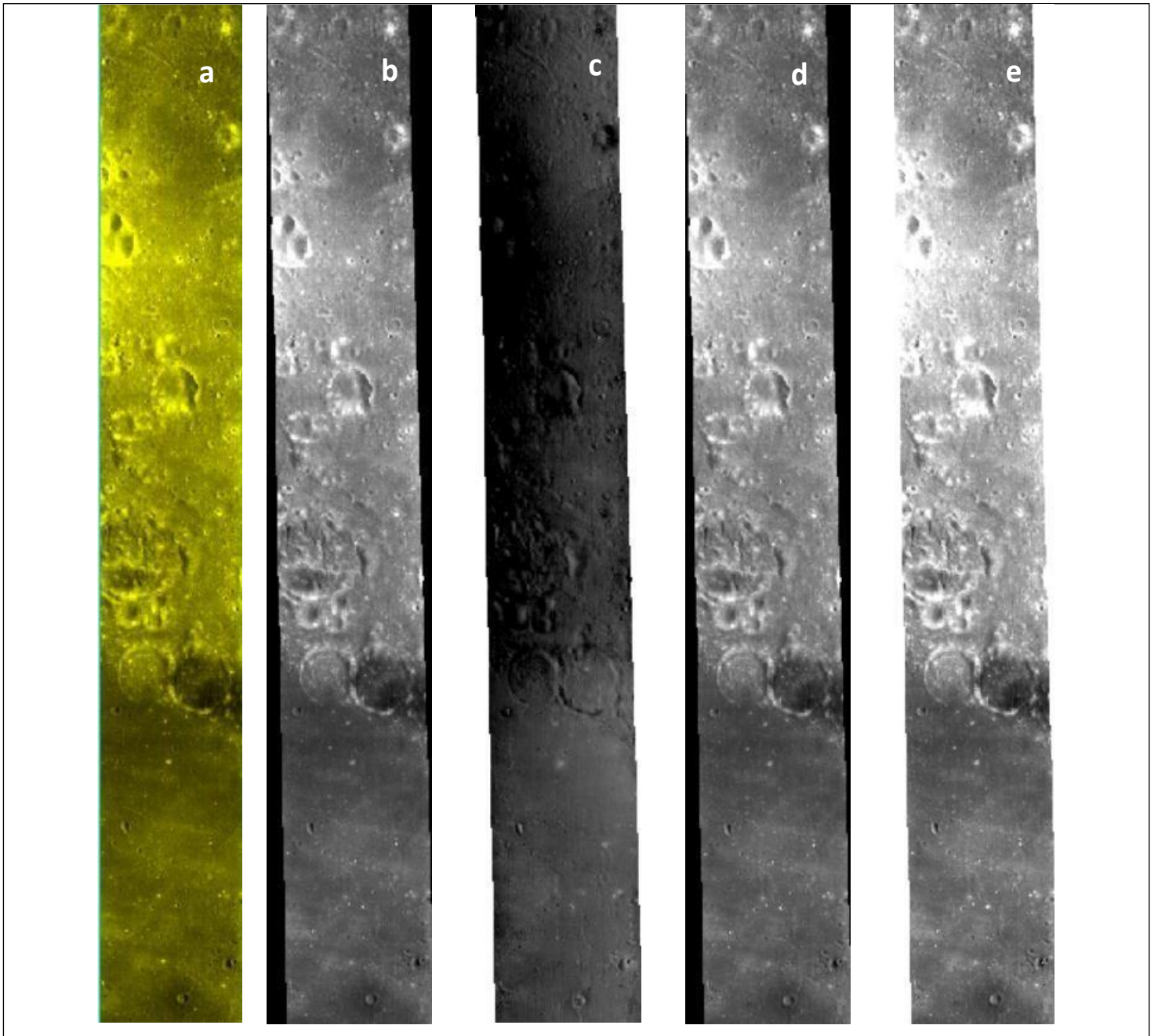


Figure 9: Different stages of preprocessing the reflectance dataset of M3. (a) Original dataset: M3G20090202T182612 (b) Georeferenced dataset (c) MNF rotation applied dataset (d) Inverse MNF applied dataset (e) Final dataset used for analysis after shadow masking.

for the quantification of absorption characteristics in the spectra. The 'continuum removal' <sup>[45]</sup> or 'convex-hull' transform is a normalisation technique that enables the comparison of spectra obtained using various equipment or in various lighting situations.

Hence, the continuum removal was employed to the extricated spectra from the calibrated M3 data. This continuum-removed spectrum highlights variations from the baseline and enhances the contrast of absorption or emission features in the data. This makes it easier to identify and

analyse the specific materials or minerals present in the scene. The operation "1 - continuum removal" is performed, using the Spectral Math tool in ENVI, after continuum removal to further enhance the spectral features of interest. In essence, it subtracts the continuum-removed spectrum from 1 (i.e., 100% minus the continuum-removed values). The purpose of this subtraction is to invert the continuum-removed spectrum, effectively highlighting the regions where the spectral features are most prominent, and emphasising areas where there are deviations from the continuum. After performing the "1 - continuum removal" operation on each band or wavelength, the data bands are summed together. This summation integrates the information across multiple wavelengths providing a more comprehensive view of the spectral features present in the data. The result is the Integrated Band Depth (IBD) map, which represents the integrated or cumulative depth of spectral features across the selected bands after continuum removal and spectral math operations.

### ***2.2.2 Integrated Band Depth (IBD)***

Integrated Band Depth (IBD) measurements at wavelengths of 1, 1.25, and 2 micron were computed to gain insights into and characterize the lunar mafic lithology<sup>[40][42][43]</sup>.

Specifically, the ones at 1.25 micron were utilized to emphasize the anorthosite lithologies<sup>[40][46]</sup>. Table 1<sup>[46]</sup> presents the formula used for calculating IBD and the corresponding absorption bands<sup>[46]</sup>, with 'R' representing the reflectance at a specific wavelength, and 'Rc' being the continuum reflectance<sup>[87]</sup> classified as a straight line across the absorption band<sup>[40][45]</sup>. To create IBD colour composites, IBD 1 micron, IBD 2 micron, and IBD 1.25 micron were allotted to the red, green, and blue channels, respectively<sup>[40][43][46][47]</sup>.

### ***2.2.3 Spectral Indices***

Applying spectral indices to data attained by M3 using remote sensing software such as ENVI (Environment for Visualizing Images) is a common

step in lunar mineralogical analysis. Spectral indices are mathematical calculations or algorithms applied to the spectral data obtained by instruments like M3 to identify and quantify the presence of specific surface properties and minerals on the lunar surface<sup>[44]</sup>. These indices are derived from the reflectance spectra of minerals, which exhibit unique

features or absorption bands in the near-infrared region. The mineral indices were generated on the grounds of relative band depth, which intensifies the absorption characteristics irrespective of the effect of topographic slope and albedo differences on the spectral variations [48][40]. When applied to M3 data, spectral indices can impart beneficial evidence about the distribution of minerals across the lunar surface[85]. Depending on the research objectives and the minerals of interest, specific mineral indices that are appropriate for the analysis are selected. Common mineral indices available that were used in lunar studies include ferrous minerals, clay minerals, water band index, modified normalised difference water index alongside the Modified Gaussian Model (MGM) and the Band Depth Ratio (BDR), among others. Each of these indices targets specific absorption features of minerals.

Measure	Equation	Definition
IBD over the 1-micron spectral region	$\sum_{n=0}^{z_0} 1 - \frac{R(790 + 20n)}{Rc(790 + 20n)}$	The cumulative band depths from 0.789 to 1.308 micron about a nearby continuum range defined from 0.699 to 1.578 micron.
IBD over the 1.25-micron spectral region	$\sum_{n=0}^{z_0} 1 - \frac{R(1029 + 20n)}{Rc(1029 + 20n)}$	The cumulative band depths from 1.029 to 1.698 micron about a nearby continuum range defined from 1.029 to 1.698 micron.
IBD over the 2-micron spectral region	$\sum_{n=0}^{z_0} 1 - \frac{R(1658 + 40n)}{Rc(1658 + 40n)}$	The cumulative band depths from 1.658 to 2.498 micron about a nearby continuum range defined from 1.578 to 2.538 micron.

Table 1: Spectral parameters that were used to assess the near-infrared absorptions defining the spectral parameters used to identify mineral [46]

Depending on the research goals and the specific surface properties or minerals of study, these appropriate spectral indices were chosen. These are designed to highlight specific features or characteristics in the reflectance spectra that are indicative of certain materials or conditions. The chosen indices were applied to the M3 data. This involves using the appropriate mathematical formulas or algorithms designed in ENVI to calculate the index values for each pixel or location on the lunar surface. After calculating the spectral indices, the results were visualised as index maps and colour composite maps. These maps represent the distribution of the specific surface properties or materials of interest across the lunar surface. The values on these maps may indicate the presence or abundance of minerals.

#### ***2.2.4 Modified Gaussian Model (MGM) Method***

In parallel with the extraction of spectral considerations such as Integrated Band Depth (IBD) and spectral indices, a further level of spectral analysis was conducted using the Modified Gaussian Model (MGM) technique<sup>[40]</sup>. M3 measures reflected sunlight at various wavelengths, and these spectra can be convoluted by the existence of multiple minerals or materials with overlapping absorption features, being the core of the MGM technique<sup>[49][50][51]</sup>. The MGM analysis aims to provide a detailed characterization of the lunar surface's mineral composition by deconvolving the complex spectral signatures, particularly those arising from overlapping absorption features. The MGM applies a mathematical model to these spectra to separate the contributions of individual minerals or materials. Even though M3 has a lower resolution and signal-to-noise ratio (SNR), it can be used to develop relative compositional knowledge through MGM analysis<sup>[52][40]</sup>.

A modified Gaussian function, `modified_gaussian` (x, amplitude, centre, width, baseline), was defined. This function served as the mathematical representation of the expected shape of spectral features and was critical for the subsequent fitting process. A specific pixel from the spectral region of interest was identified within the M3 data, which is the pixel with geographic coordinates 9° 25 '58.86" N and 38° 40' 9.00" E latitude and longitude respectively. This region was carefully chosen based on the spectral features that were to be analysed and was defined by wavelength boundaries. Initial estimates for the parameters of the modified Gaussian function, including amplitude, centre (peak position), width (spread), and baseline (background), were provided. These initial estimates were determined based on the nature of the spectral features being investigated. The modified Gaussian function was fitted to the selected spectral data within the specified pixel. This fitting process was performed using the `curve_fit` function from the SciPy library. The objective was to estimate the parameters that best described the spectral feature, thus enabling its deconvolution.

The success of the MGM analysis was assessed through the calculation of the R-squared (Coefficient of Determination) value. This statistical metric provided a measure of how effectively the fitted modified Gaussian curve represented the original spectral data. A higher R-squared value indicated a better fit and thus increased confidence in the results. Validation of the MGM analysis results was essential to ensure the accuracy and reliability of the mineral composition estimates. This validation process involved comparisons with known spectral features, laboratory measurements, or ground truth data, where available.

### 2.2.5 Mineral Indices

In this study, mineral indices were employed as a supplementary method to identify the existence of pyroxene, spinel, and ferroan anorthosite. These indices rely on specific ratio parameters, known as the pyroxene ratio, spinel ratio, and PAN ratio (Table 2)<sup>[40][52]</sup>.

These mineral indices operate based on relative band depth, which magnifies the absorption features observed in the data while mitigating the influence of topographic slope and albedo differences on spectral variations<sup>[40][53]</sup>. The PAN and pyroxene ratios were calculated by dividing the reflectance values observed at the shoulder of absorption by the reflectance minima values occurring within the absorption region<sup>[40]</sup>. For pyroxene, the reflectance minimum is found at a wavelength of 0.95 micron, whereas for lunar plagioclase, it occurs at 1.25 micron<sup>[40]</sup>. Spinel, on the other hand, exhibits absorption in the vicinity of the 2 micron region, but the longer wavelength shoulder of this absorption is not evident in the M3 dataset<sup>[40]</sup>. Consequently, for the spinel ratio, the numerator consists of the reflectance value observed at the shorter wavelength shoulder of the absorption.

These mineral ratios are then employed to produce a colour composite image in which red, green, and blue channels correspond to the ratios of pyroxene, spinel, and PAN, respectively<sup>[40]</sup>. This composite image aids in visually identifying and distinguishing the mineralogical variations in the dataset.

Mineral index	Formula Used	RGB colour denoted
Pyroxene ratio	$(R_{700} + R_{1200}) / 2 * R_{950}$	Red
Spinel ratio	$R_{1400} / R_{1750}$	Green
PAN ratio	$(R_{1000} + R_{1500}) / 2 * R_{1250}$	Blue

Table 2: Band ratio formula and colour assigned for deriving the spectral parameters

### 2.3 CLASS

CLASS measures the Moon's X-ray Fluorescence (XRF) spectra to inspect the existence of major elements such as Sodium, Magnesium, Aluminium, Silicon, Calcium, Titanium, and

Iron,. The XRF technique identifies these elements by determining the characteristic X-rays they emanate when excited by solar X-ray emission<sup>[54]</sup>. CLASS being a non-imaging spectrometer, consists of sixteen SCDs that are time-tagged events defining the field of view of each detector as 7 deg X 7 deg Full Width at Half Maximum (FWHM)<sup>[54]</sup>. This translates to a 12.5 km X 12.5 km footprint at the 100 km altitude of the spacecraft<sup>[54]</sup>. For each SCD, this is binned to an 8-second spectrum. The time it takes to travel 12.5 kilometres over the surface of the moon is equal to 8 seconds. To create a single 8s combined spectrum, the individual SCD spectrum is re-binned in energy space after being compensated for the temperature-dependent gain<sup>[20]</sup>.

### ***2.3.1 Data Extraction and Preprocessing***

The primary data source for this study consisted of Level 1 FITS files obtained from the CLASS (Chandrayaan 2 Large Area Soft X-ray Spectrometer) instrument, part of the PRADAN (Planetary Radars for the Detection of Asteroids and Near-Earth Objects) project. These files contained X-ray Fluorescence (XRF) spectral data, capturing the interactions between the instrument and the target elements, particularly Mg, Al, and Si lines. The FITS files were loaded using the `astropy.io.fits` Python library to provide the basis for further analysis. The data arrays were then extracted, containing information about channels and their corresponding counts.

The initial focus was on identifying the XRF signals related to the Mg, Al, and Si lines to isolate the elements of interest. These XRF lines may or may not be seen in an 8-second spectrum depending on the solar flare's intensity, season (NM/DD), geometry, and composition. The single 8s integrated FITS file downloaded did not contain significant XRF lines. To address this issue, the spectra may be added to improve statistics which is a simple addition in time. Based on the strength of the signal, the data from two files (continuous in time) were combined to create a comprehensive and representative spectrum, making it a 16s window.

### ***2.3.2 XRF Signals Identification***

After the addition of the files, the focus was on identifying the specific XRF signals<sup>[55]</sup> related to the Mg, Al, and Si lines. To ensure a robust dataset, two distinct approaches were



adopted. The first involved confirming the presence of these signals within a 16-second time window (the added two files each being 8-second) in the spectra. The second approach leveraged the occurrence of solar flares to filter and extract specific L1 files. These two methodologies ensured the inclusion of significant signals while mitigating noise. Spectra visualisation was crucial for understanding the distribution and characteristics of the XRF signals. It allowed for an initial assessment of the presence and intensity of the desired XRF signals in the spectra.

### ***2.3.3 Baseline Correction***

A Gaussian peak fitting approach was employed to model the identified peaks corresponding to Mg, Al, and Si lines. Employing Gaussian peak fitting to model the identified peaks, aids in precise parameter extraction. The parameters, which are, amplitude, mean (centroid), and standard deviation (width), are vital for understanding the characteristics of the signals. A custom peak-fitting algorithm was implemented to address cases of peak overlap and ensure accurate parameter extraction. A rolling ball baseline correction technique was applied to mitigate background noise and enhance the clarity of the peaks.

Rolling ball baseline correction is a data preprocessing technique commonly used in analytical chemistry, particularly in spectroscopy and chromatography, to remove baseline drift or fluctuations from a signal. Baseline drift can obscure the true features of a spectrum or chromatogram and affect the accuracy of data analysis. The rolling ball baseline correction method helps to correct this issue by estimating and subtracting the baseline from the data.

The correction works as follows:

1. **Data Acquisition:** Acquiring the raw data, which in this case is a spectrum (channels vs counts).
2. **Define the Rolling Ball:** Choosing a window size called the "rolling ball." This window is essentially a moving average window that will slide along the data. The size of the rolling ball is determined based on the characteristics of the data and the baseline drift needed to correct. A larger rolling ball size will correct for broader baseline fluctuations, while a smaller size will correct for finer fluctuations.

3. **Moving Average:** The rolling ball window is moved along the data points, and for each position, a moving average is calculated within the window. This moving average represents an estimate of the local baseline.
4. **Subtraction:** The calculated moving average is subtracted from the original data point at the centre of the rolling ball window effectively removing the estimated baseline from that point.
5. **Iterative Process:** Steps 3 and 4 are repeated for each position along the data. The rolling ball window moves sequentially along the entire dataset.
6. **Baseline-Corrected Data:** After processing the entire dataset, a baseline-corrected version of the data is obtained, where the baseline fluctuations have been removed.

Rolling ball baseline correction is particularly useful when dealing with data from instruments that may introduce baseline drift due to variations in background signal, noise, or other external factors <sup>[56]</sup>. It helps improve the accuracy of peak detection, integration, and subsequent data analysis.

#### ***2.3.4 Gaussian Peak Fitting***

The baseline-corrected spectrum provided a clear representation of the peaks of interest. The peaks were identified based on their prominence within the baseline-corrected spectrum. For a comprehensive understanding, data points were extracted around each peak using a specified window size. The resulting data points were plotted to provide a visual representation of the peaks and their surroundings. The culmination of the methodology involved a comprehensive analysis of the rebinned and baseline-corrected spectra. Gaussian fits provided insights into the characteristics of the identified peaks. These fits were visually assessed alongside the original baseline-corrected data and the extracted peaks. Sigma values were calculated and marked on the plots, aiding in the assessment of peak significance and distribution.

## **2.4 IIRS**

IIRS is an imaging hyperspectral tool used to analyse the mineralogy of the lunar surface, including the hydroxyl signature. CIIRS functions with roughly 256 contiguous bands in the

spectral range of 0.8–5 micron. At a height of 100 km on a polar circular orbit, IIRS detects the reflected solar radiation in addition to the emissions from the lunar surface. With a spatial resolution of around 80 m and a spectral resolution of about 20–25 nm spanning the spectral range of 0.8–5.0  $\mu\text{m}$  in about 250 spectrally continuous bands, it has an 80 m ground sampling distance (GSD) and a 20 km swath at nadir<sup>[54]</sup>. The spectrometer can identify the diagnostic absorption features of both major and minor lunar minerals since they appear in the  $\sim 0.75\text{--}2.5$   $\mu\text{m}$  spectral domain, which is well within the IIRS spectral range<sup>[54]</sup>. On the other hand, the spectral range of  $\sim 2.5\text{--}3.3$   $\mu\text{m}$ <sup>[54]</sup> was being devotedly used to detect the occurrence of lunar OH/H<sub>2</sub>O features having fundamental absorptions around 3.0  $\mu\text{m}$ <sup>[54]</sup>. The datasets were downloaded from the PRADAN website. The Mare Tranquillitatis region was covered by IIRS and saved in files with the labels: ch2\_iir\_nci\_20220112T2126203147\_d\_img\_hw1, ch2\_iir\_nci\_20220112T2120452496\_d\_img\_hw1, ch2\_iir\_nci\_20210719T1538509046\_d\_img\_d32, ch2\_iir\_nci\_20210719T1340522043\_d\_img\_d32, ch2\_iir\_nci\_20210719T1142532037\_d\_img\_d32, ch2\_iir\_nci\_20210719T0944545715\_d\_img\_d32\_no, ch2\_iir\_nci\_20210621T2245238783\_d\_img\_hw1

#### ***2.4.1 Data Extraction and Georeferencing***

The georeferencing of remote sensing data is a critical step in transforming raw satellite images into geospatial information that can be analysed and interpreted in the context of the Earth's surface. Georeferencing ensures that pixel coordinates in the data are accurately linked to corresponding geographic coordinates on the lunar surface. Apart from the raw data file, the downloaded dataset also contained a geometry folder with a CSV file containing the geometry details including longitude, latitude, pixel, and scan values, which were essential for accurate georeferencing.

The georeferencing process was done by importing the necessary Python libraries, including pandas for data handling and rasterio for working with raster data. The CSV file containing geometry details is then read. Simultaneously, the raw IIRS data is imported using rasterio. The methodology calculates the pixel size and resolution based on the provided geometry details and the original raster's dimensions, assuming a uniform grid. A new transformation matrix, `new_transform`, was generated with these values. Subsequently, the metadata of the georeferenced data was updated to incorporate the new transformation matrix, width, height,

and CRS. Finally, the georeferenced data was written to a new .qub file, preserving spectral information in separate bands. The result was a georeferenced dataset that could be effectively analysed and interpreted in a geospatial context using GIS software.

### ***2.4.2 Data Preprocessing***

After georeferencing the IIRS data, the following series of data processing steps and analyses were performed, with the help of ENVI software to enhance data quality and extract meaningful information for lunar surface studies. Initially, an MNF transformation was applied to the georeferenced data. MNF is a technique that reduces noise and highlights the most informative spectral features within hyperspectral data. By applying MNF, the data's signal-to-noise ratio was improved, enhancing spectral clarity and feature discrimination.

After the MNF transformation, an Inverse MNF was employed. This step reverted the data to its original space while preserving the noise reduction benefits achieved through MNF. This allowed for a more meaningful interpretation of the spectral information. Shadow masking techniques were implemented to address the impact of shadows and varying illumination conditions on the spectral data. These techniques identified and masked out areas affected by shadows, ensuring that subsequent analyses were based on reliable and shadow-free data.

The spectral data pre-processed thus far exhibited thermal disturbances that required correction. Thermal correction techniques were applied to account for temperature variations and emissivity effects across the lunar surface. These corrections helped in producing temperature-compensated spectral information for accurate analysis. Specific regions of interest (ROIs) were defined and extracted from the larger dataset. By focusing on ROIs, computational efficiency was improved, and the analysis was directed towards areas of particular scientific interest or relevance.

### ***2.4.3 IBD and Spectral Analysis***

IBD maps were generated at critical spectral wavelengths, including 1-micron, 2-micron, and 3-micron <sup>[43][46][47]</sup>. These maps provided valuable insights into variations in brightness and darkness across the lunar surface. Such variations often correlate with different surface materials and compositions, making IBD maps a crucial tool for lunar surface

characterization. Spectral indices were computed, including the clay index, ferrous index, and water band index <sup>[48]</sup>. These indices offered quantitative measures of key surface properties, such as mineral composition and the presence of water or hydrated materials. They were used to identify and map specific surface features and materials. Band ratio plots were created to visualise the relationships between different spectral bands. Band ratios highlight specific spectral features or absorption bands associated with certain minerals or materials. These plots enabled the identification and mapping of such features, aiding in mineralogical and compositional analysis.

In summary, the post-georeferencing data processing and analysis procedures encompass a comprehensive effort to enhance data quality, mitigate noise and illumination issues, correct for thermal disturbances, and derive valuable information about the lunar surface. These steps are instrumental in achieving accurate and scientifically meaningful results in the study of Chandrayaan-2's IIRS data and lunar surface characterization.

---

## CHAPTER 3: RESULTS

---

### 3.1 M3

#### *3.1.1 Exploration of colour composite of IBD*

The IBD (Integrated Band Depth) colour composite outputs generated by the assignment of RGB (Red, Green, Blue) colours to IBD values at 1-micron, 2-micron, and 1.25-micron wavelengths, as depicted in Figure 10, effectively conveying the compositional intricacies inherent to the study locale. The specific colouration exhibited by mafic minerals within this spectral canvas is contingent upon the relative strengths of ferrous bands, a phenomenon that arises due to disparities in the mineralogical constitution and optical maturity<sup>[52]</sup>.

Upon a perusal of the colour composites, the blue tinge assumes the role of a sentinel, denoting highland anorthitic plagioclase characterised by subdued mafic absorptions. In contrast, the presence of yellow/green to orange/red pigments within the spectrum implies the prevalence of mafic mineralogies<sup>[42][46][57]</sup>. It is worth highlighting that distinct minerals manifest varying intensities across the IBD spectrum: olivine prominently exhibits high values for IBD at 1-micron, plagioclase corresponds to elevated IBD values at 1.25-micron, spinel attains its zenith in IBD at 2-micron, while pyroxene registers notable peaks in both IBD at 1-micron and IBD at 2-micron.

A detailed examination of the IBD colour composite imagery, prominently illustrated in Figure 10, elucidates that a predominant swath of the image is enveloped in a soothing blue gradient, emblematic of the feldspathic region that typifies the geographical terrain under scrutiny. This indicates the predominant presence of ancient anorthositic minerals. However, amidst this royal azure expanse, discerning eyes may discern patches of yellow, green, and red, lending a chromatic dimension to the predominantly blue canvas. However, one can also notice streaks of yellow, green, and red among this royal azure expanse, adding chromatic complexity to the predominantly blue canvas. The presence of the yellow hue conveys the existence of a mineral with pronounced IBD values at both 1-micron and 2-micron, a hallmark feature of pyroxene. Meanwhile, the verdant shades allude to the dominance of IBD

at 2-micron, characteristically associated with spinel, an observation of novel significance for this particular region, hitherto unreported in extant literature.

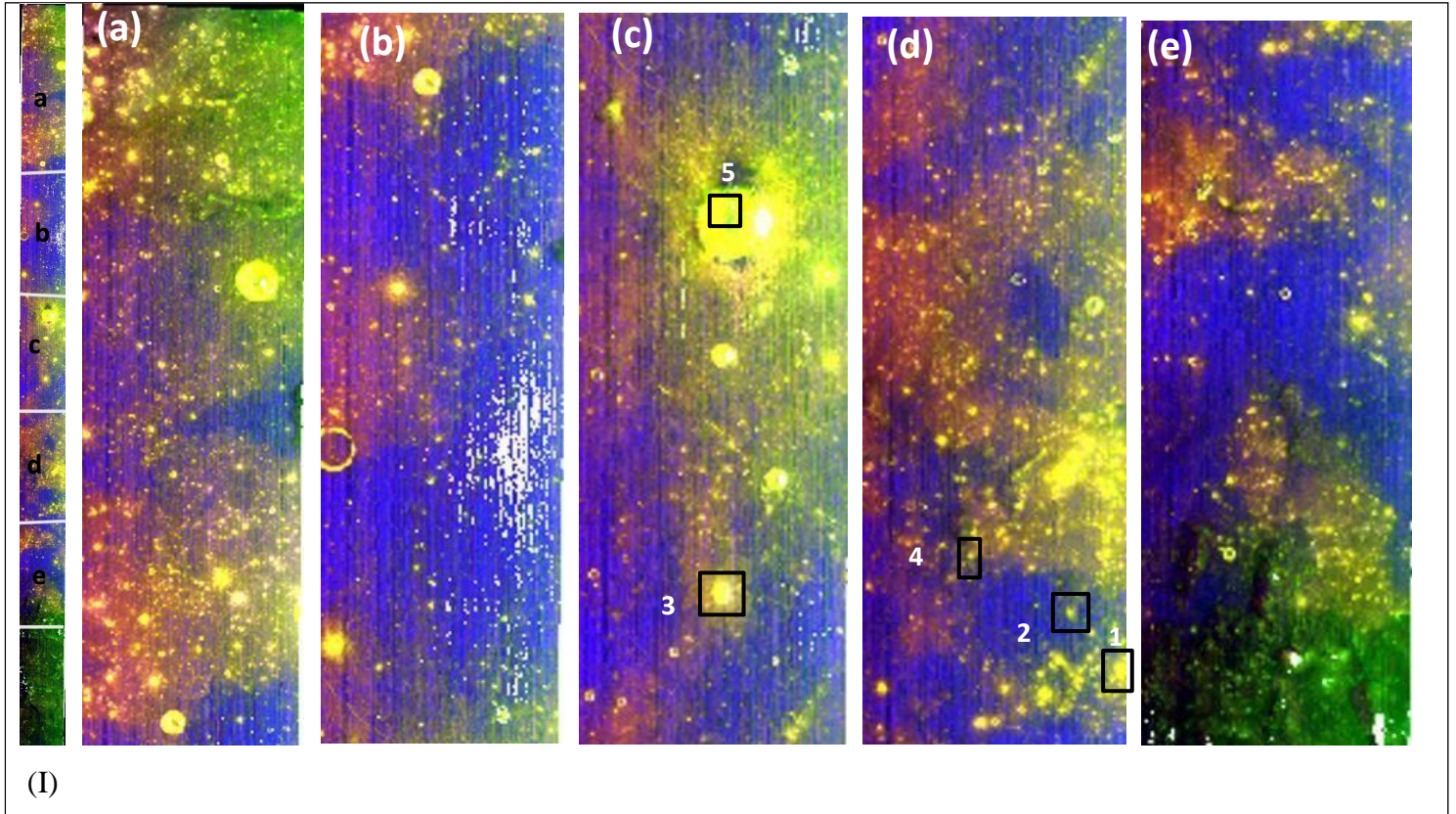


Figure 10: Colour composite produced from Integrated Band Depth (IBD) conditions of the M3 dataset M3G20090202T182612. (a), (b), (c), (d) and (e) are the zoomed-in views of the regions marked as a, b, c, d, and e respectively in Figure (I)

Colour	Region prominent with IBD
Red	1-micron
Green	2-micron
Blue	1.25-micron
Yellow (Red + Green)	1-micron and 2-micron
Magenta (Red + Blue)	1-micron and 1.25-micron
Cyan (Green + Blue)	1.25-micron and 2-micron

Table 3: Interpreting the colour composite created from IBD parameters.<sup>[40]</sup>

### 3.1.2 Exploration of Colour Composite of the Mineral Indices

The investigation entailed a comprehensive examination of mineral characteristics utilising spectral parameters and derived mineral indices, which were subsequently utilised to create a colour composite image. This endeavour served as a means to validate the mineralogical interpretations derived from the IBD (Integrated Band Depth) colour composite. Specifically, the colour composite consisted of three channels: R (Red) corresponding to the Pyroxene Ratio, G (Green) indicating the Spinel Ratio, and B (Blue) signifying the PAN (Pyroxene-Associated Neutron) Ratio, as illustrated in Figure 11.

In this meticulously constructed colour composite, distinct colours were employed to convey specific mineralogical information. Notably, regions were dominantly characterised by a pinkish-magenta shade. The magenta colour (a combination of red and blue) in this colour composite is typically associated with a high abundance of the orthopyroxene mineral.

Orthopyroxene is a group of minerals that are typically found in mafic rocks and can be associated with volcanic or basaltic compositions. The specific ratio used in the red channel (Pyroxene ratio) may be designed to highlight the presence or abundance of orthopyroxene in the analysed area. Magenta in the composite image indicates areas where this mineral or its related compositions are predominant. It is to be also noted that there are also green shades in the colour composite indicating the existence of minerals based on Spinel.

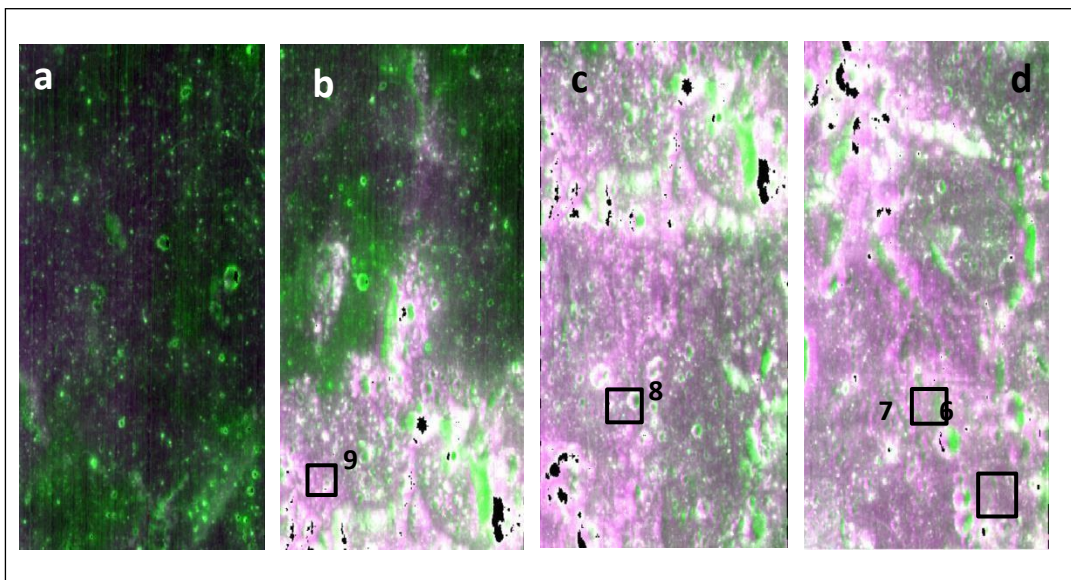


Figure 11: Mineral indices colour composite processed from Spectra conditions mentioned in Table 2, for the datasets M3G20090202T182612. R, G and B are assigned to pyroxene, spinel and PAN ratios respectively. a, b, c and d represent different regions of the dataset M3G20090202T182612



### ***3.1.3 MGM Spectral Studies***

The confirmation of mineral compositions is established through a meticulous examination of the spectral characteristics exhibited by pixels equating to the distinctive colours within the colour composites. The positions at which these spectra were acquired are demarcated by square boxes in Figures 10 & 11.

Spectra no.1, as depicted in Figure 12, manifests absorptions at both 1-micron and 2.1 micron. The absorption feature at 1-micron was wide and demonstrated a discernible imprint of the 1.25-micron absorption<sup>[40]</sup>. Likewise, the 2.1-micron feature exhibited a broad absorption pattern, with its absorption depth surpassing that of the 1-micron feature. Spectra no.3, also depicted in Figure 12, shares similarities with Spectra no.1, albeit with the distinction that the absorption feature at 2-micron was shallower in comparison to the 1-micron feature<sup>[40]</sup>.

A marked departure from Spectra no.1 and 3 is observed in Spectra no.2. In this instance, the absorption centres were located at 0.95 micron and 2.1 micron, with significantly lower intensities than those seen in Spectra no.1 and 3. Moreover, a shallow 1.25-micron absorption feature, characteristic of the ferroan anorthosite, was discernible. Spectra no. 4 and 5 also display absorptions at 0.95 micron and 1.25-micron, along with a shallow, broad feature at 1.95 micron. Spectra no. 6 to 9, as illustrated in Figure 13, diverged from the aforementioned patterns by exhibiting either no or minimal absorption features at 1-micron. Instead, they prominently showcased absorption features<sup>[40]</sup> around 2-micron (for Spectra no. 6) and 2.1 micron (for Spectra no. 7 to 9).

Further insights were gleaned when examining the band centres derived from the M3 data for Spectra no. 1 and 3. These spectra deconvolved into four absorption bands each, as illustrated in Figure 15 and detailed in Table 4<sup>[40]</sup>. These deconvolved bands encompassed the band1 centre (B1C) representing the 1-micron band, situated at approximately 0.98-micron; the band2 centre (B2C) positioned around 1.2micron; the band3 centre (B3C) coinciding with the 1.9-micron band; and the band4 absorption centre (B4C) situated at 2.2-micron. This deconvolution suggested the presence of multiple mineralogical components contributing to the composite spectra of Spectra no. 1 and 3.

In the case of Spectra no. 2, 4 and 5, they exhibited the potential for deconvolution into five absorption bands each, as shown in Figure 16 and outlined in Table 5<sup>[40]</sup>. These bands

included the band centre 0 (BC0) at 0.7-micron. Spectra no. 4 and 5 each display two absorption bands around 1-micron and two additional bands around 2-micron. The shorter wavelength absorption band for 1-micron, denoted as band centre 1 (BC1), is positioned at 0.95-micron, while for the 2-micron region, the band centre 3 (BC3) is located at 1.8-micron. Conversely, the longer wavelength absorption band centre<sup>[40]</sup> for the 1-micron region, referred to as band centre 2 (BC2), is centred at 1.2-micron, and for the 2-micron region, the band centre 4 (BC4) stands at 2-micron. This complex deconvolution suggests intricate mineralogical composition within Spectra no. 4 and 5.

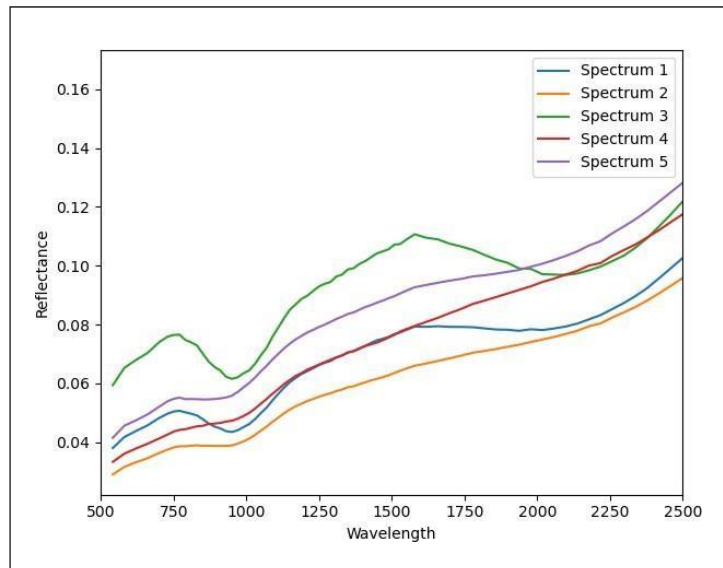


Figure 12: Spectra of various pyroxene exposures. There is a clear distinction between the two main lunar pyroxenes. The high Ca pyroxene spectra, represented by spectra 1 and 3, have 1-micron and 2-micron absorption positions at longer wavelengths than the low Ca pyroxene spectra, which are represented by spectra 2, 4 and 5. Figs. 10 and 11 show the positions of the extracted pixel area.

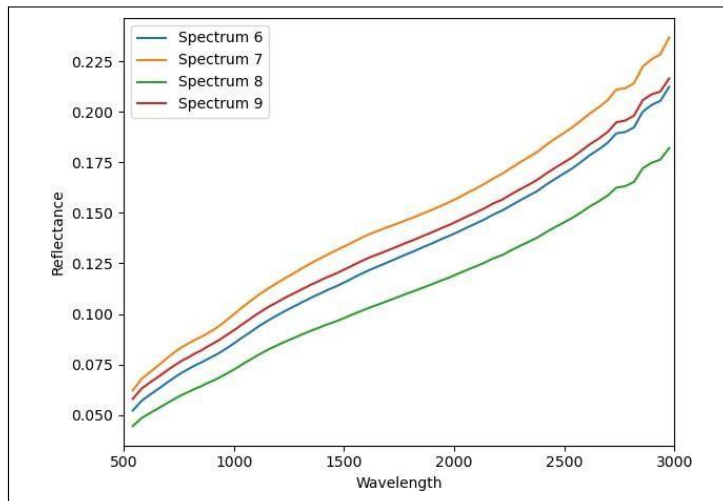


Figure 13: Spectra of various spinel exposures with a strong and broad 2-micron absorption. The band centre of 2-micron position is at wavelengths longer than 2-micron. This indicates the presence of Mg-Spinel in the area. The locations of the extracted spectra are marked in Figs. 10 and 11

### 3.1.4 Exploration of Colour Composite of the Spectral Indices

The derivation of lunar mineralogical insights was meticulously conducted through the utilisation of the Spectral Indices tool within the ENVI software. This analytical approach yielded the creation of specialised thematic maps showcasing the spatial distribution of key lunar minerals and indices: ferrous minerals, clay minerals, and the water index. Each of these elements was assigned to distinct spectral bands, enabling the generation of a comprehensive colour composite representation that illuminates the lunar surface's mineralogical tapestry. The resultant colour composite is a visually compelling representation where each constituent mineral and index are uniquely conveyed by distinct hues.

Specifically, the colour schema employed consisted of Red (R) signifying ferrous minerals, Green (G) indicating clay minerals, and Blue (B) representing the water index.

In this context, the colouration observed in the resulting composite predominantly assumes a pink or magenta hue (Figure 14). This striking magenta colour predominantly corresponds to regions enriched in ferrous minerals, where the vibrant red colouration serves as a visual marker for the presence of these significant lunar constituents. The identification and mapping of ferrous minerals are of paramount importance in lunar science as they offer valuable insights into the geological history and processes that have shaped the lunar landscape.

Moreover, the composite image also reveals the presence of distinct green patches (Figure 16), frequently encircled by yellow areas, which tend to be associated with specific topographic features on the lunar surface such as craters or pits. The green colouration signifies the presence of clay minerals, a pivotal discovery that holds implications for our understanding of lunar geology. These clay minerals may provide critical clues about the geological evolution of the Moon and the interplay of various processes that have shaped its surface. The surrounding yellow regions may suggest a transitional zone, highlighting the complexity of mineralogical compositions at the boundaries between different geological features.

Spectra Id	Band1 Centre (BC1) in nm	Band2 Centre (BC2) in nm	Band3 Centre (BC3) in nm	Band4 Centre (BC4) in nm	R-squared value
1	930.2648	1222.5617	1902.0606	2126.4098	0.9942
3	946.8243	1211.9785	1932.3316	2188.5115	0.9940

Table 4: Band centres derived from MGM for Spectra no. 1 and 3

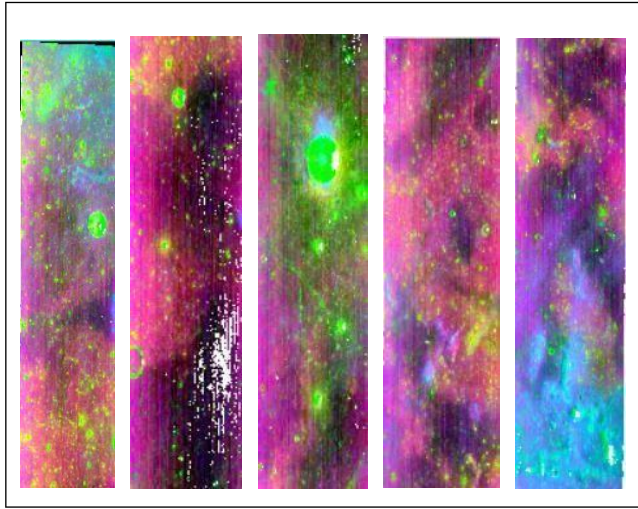


Figure 14: Spectral indices colour composite generated from the M3 dataset M3G20090202T182612. a, b, c, d, and e are zoomed-in versions of the region of study

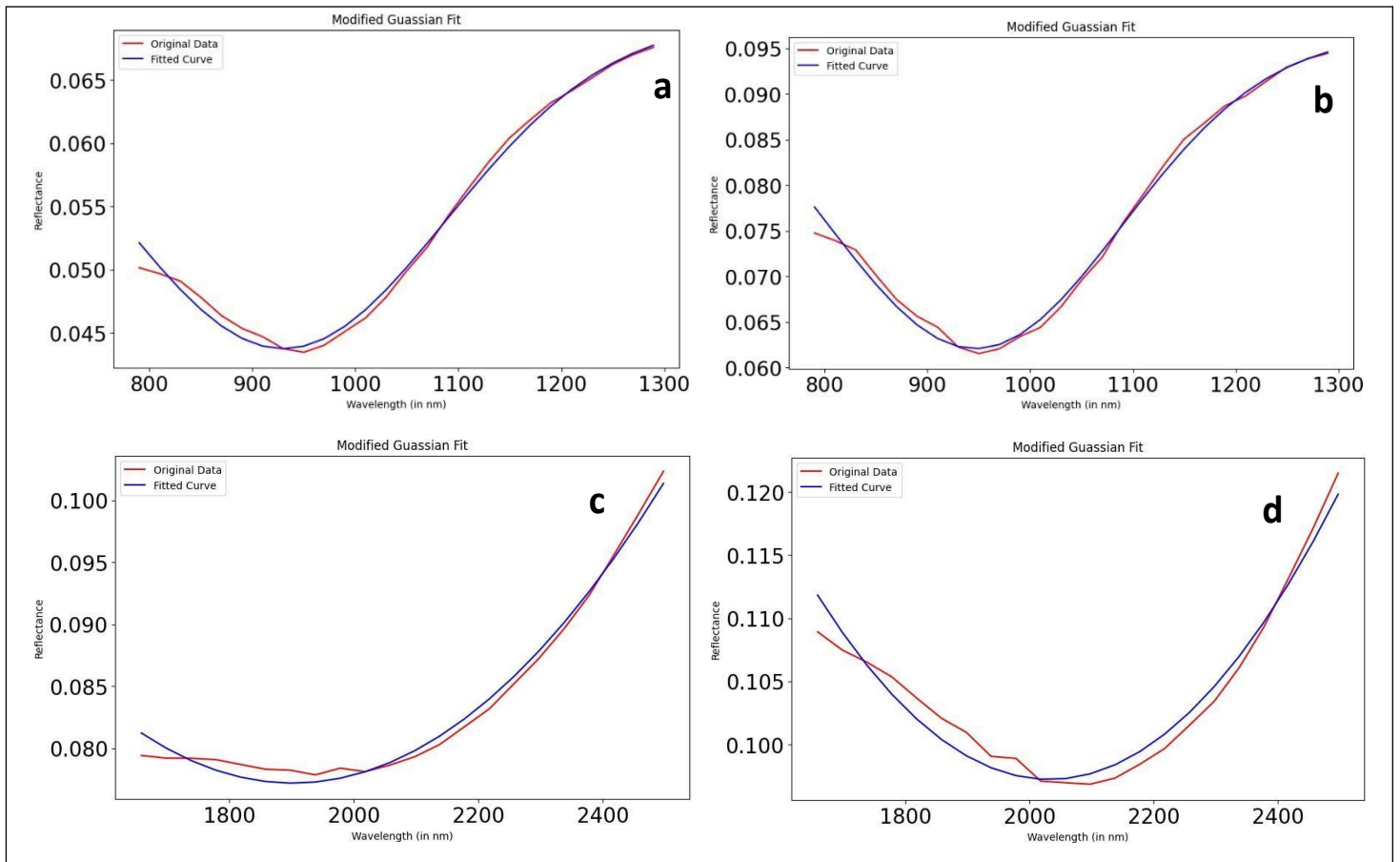


Figure 15: Modified Gaussian Model applied to Spectra 1 and 3 at 1000 and 2-micron indicating the presence of a High-Ca pyroxene (X-axis: Wavelength in nm, Y-axis: Reflectance). (a) and (c) are the MGM-derived Gaussians of spectra no. 1 at 1-micron and 2-micron respectively. (b) and (d) are the MGM-derived Gaussians of spectra no. 3 at 1000 and 2-micron respectively.

Spectra Id	Band0 Centre (BC0) in nm	Band1 Centre (BC1) in nm	Band2 Centre (BC2) in nm	Band3 Centre (BC3) in nm	Band4 Centre (BC4) in nm	R-squared value
2	837.0081	927.6644	1220.9380	1827.6095	2093.9266	0.9959
4	888.7660	917.8321	1225.0793	1842.9265	2049.6609	0.9975
5	821.4516	905.0703	1235.1793	1802.0414	2052.3715	0.9869

Table 5: Band centres derived from MGM for Spectra no. 2, 4 and 5

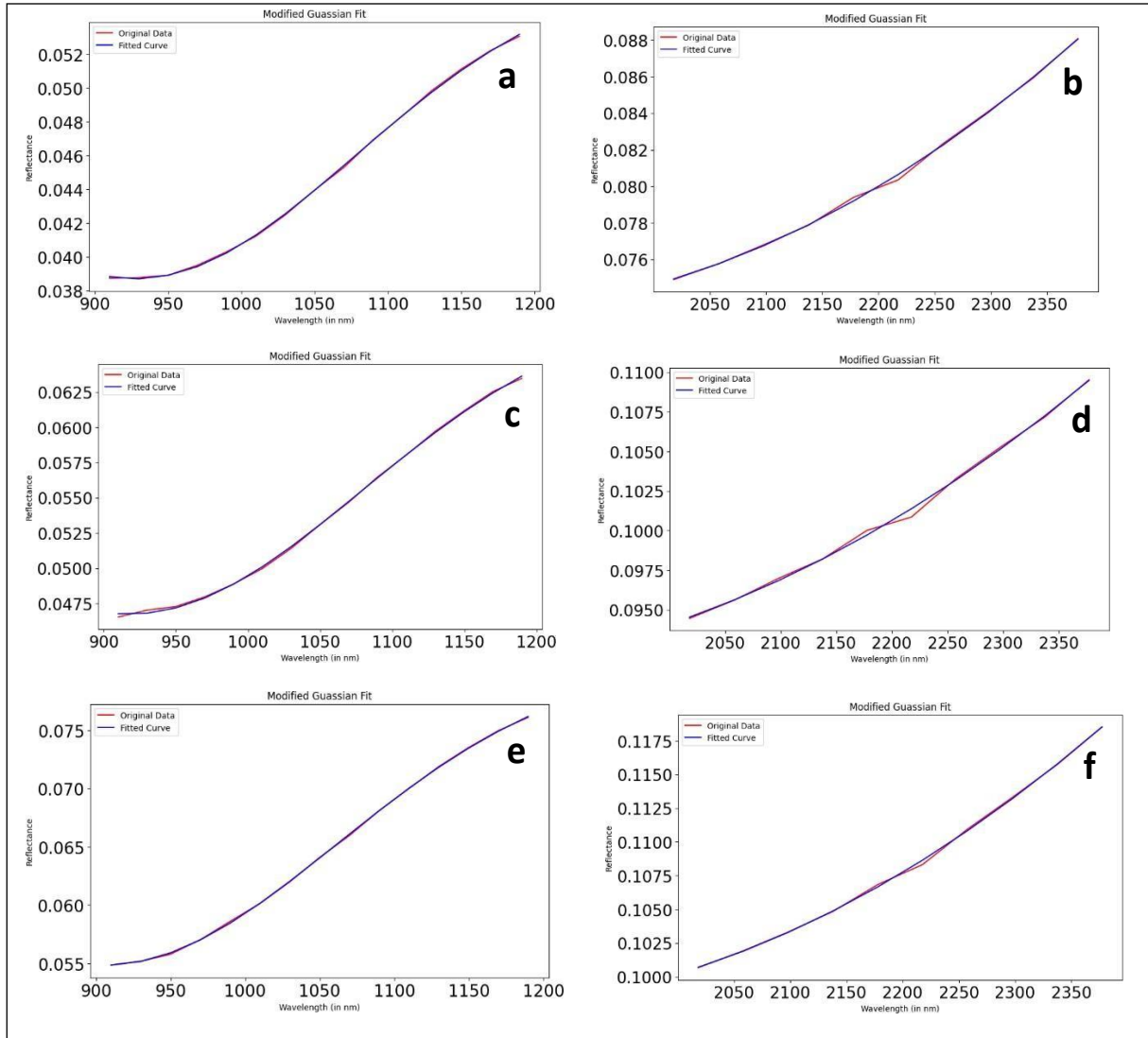


Figure 16: Modified Gaussian Model applied to Spectra no. 2, 4 and 5 at 1000 and 2-micron indicating the presence of a Low-Ca pyroxene (X-axis: Wavelength in nm, Y-axis: Reflectance). (a) and (b) are the MGM-derived Gaussians of spectra no. 2 at 1-micron and 2-micron respectively. (c) and (d) are the MGM-derived Gaussians of spectra no. 4 at 1000 and 2-micron respectively. (e) and (f) are the MGM-derived Gaussians of spectra no. 5 at 1000 and 2-micron respectively.

### 3.2 IIRS

### ***3.2.1 Exploration of Colour Composite of IBD***

The IBD (Integrated Band Depth) colour composite outputs derived from the assignment of RGB (Red, Green, Blue) colours to IBD values at specific wavelengths for the IIRS dataset, offer an insightful representation of the compositional intricacies within the study area. These colour composites reveal critical details about the distribution of distinct mineralogical components, unveiling their unique spectral signatures and relative strengths, thereby enhancing our understanding of the geological makeup<sup>[52]</sup>.

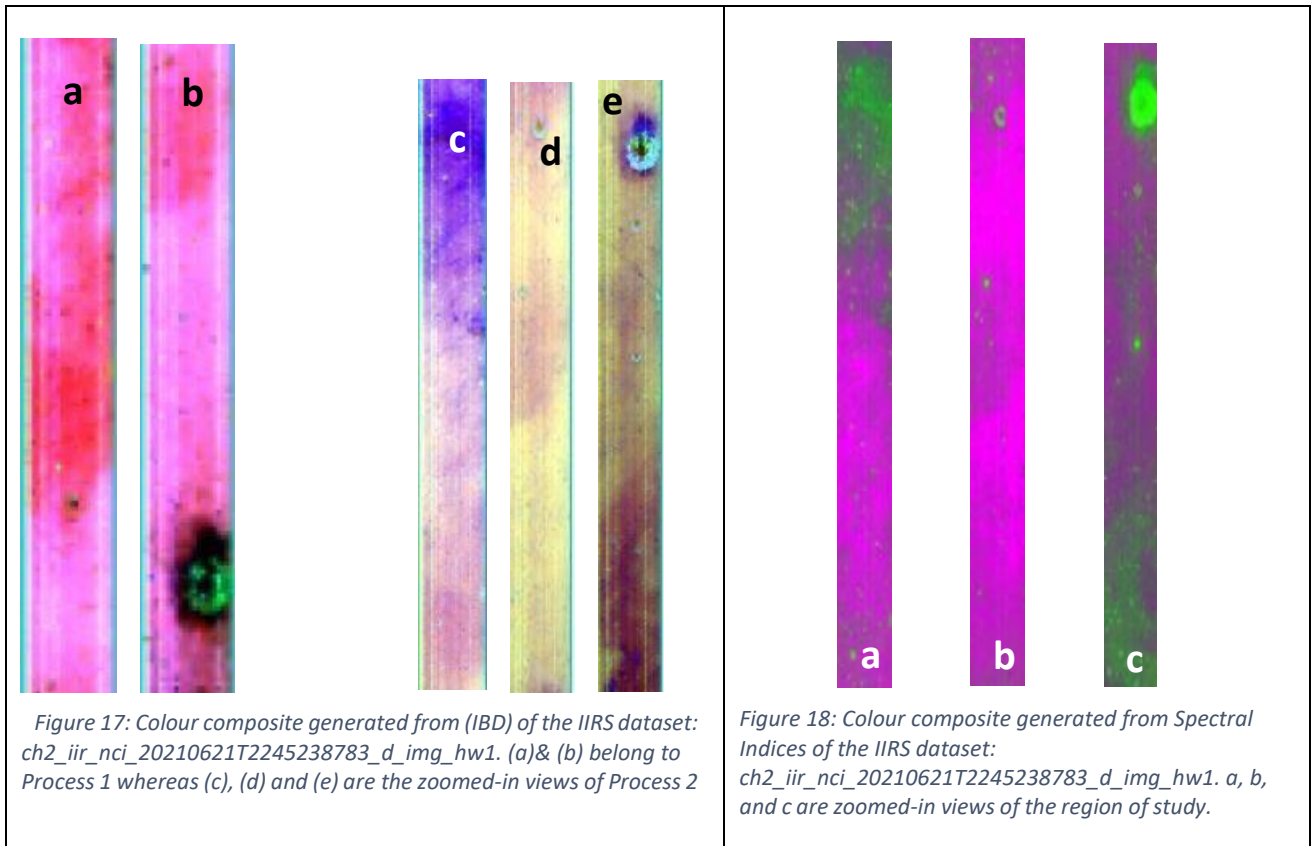
In the examination of the IBD colour composites, we first consider the results of Process 1 (Figure 17), where R (Red) corresponds to IBD1000, G (Green) to IBD2000, and B (Blue) to IBD1250. The dominant pinkish-magenta colouration observed in this composite signifies the prevalence of the pinkish-magenta colour i-e- strong absorption around 1-micron and 1.25-micron within the study area. The green patches, which often accompany the red areas, provide valuable insights into the presence of additional mineralogical variations with absorption at 2-micron. These green regions typically correspond to specific geological features or alterations in elemental composition, adding a layer of complexity to the predominantly red colour scheme.

Moving on to Process 2, where R (Red) represents IBD1000, G (Green) represents IBD2000, and B (Blue) represents IBD3000, the resulting purple IBD map presents a distinctive colour palette. Within this composite, maroon and yellow patches emerge as prominent features, each conveying unique mineralogical information. The maroon regions indicate the dominance characterised by spectral signatures at 1-micron wavelengths, highlighting their prevalence within the study area. Conversely, the yellow patches suggest the presence of alternative elemental compositions or variations in the geological makeup, creating a visually striking contrast against the purple backdrop.

### ***3.2.2 Spectral Indices Colour Composite Analysis***

The colour composite maps generated through the utilisation of the Spectral Indices tool within ENVI, specifically focusing on the Ferrous, Clay, and Water Index maps derived from the IIRS dataset, provide valuable insights into the mineralogical and compositional characteristics of the lunar surface. In this colour composite representation, a deliberate colour scheme was employed to encode the distinct spectral information related to ferrous minerals, clay minerals, and the water index. Red (R) was assigned to represent Ferrous

minerals, Green (G) denoted Clay minerals, and Blue (B) signified the Water Index. This colour coding was strategically chosen to facilitate the intuitive interpretation of the mineralogical data, offering a clear visual language to understand the distribution of these vital geological components.



The resulting colour composite predominantly manifests as a striking pink or magenta hue, which signifies the prevalence of Fe-based mineral types across the lunar terrain (Figure 18). The pink/magenta shade serves as a visual marker for regions enriched in Ferrous minerals, as indicated by the spectral index colour composite from the data recorded by M3(Figure 14). The presence of Ferrous minerals, often associated with iron-bearing compounds, is a critical aspect of lunar geology, providing valuable clues about the geological history and processes that have shaped the Moon.

The green patches are indicative of the presence of Clay minerals (Figure 18), representing a significant discovery within the lunar surface. Clay minerals have the potential to offer essential insights into the geological evolution of the Moon and the complex interplay of various geological processes that have left their mark on the lunar landscape.

### 3.3 CLASS

The analysis of the Level 1 FITS files acquired from the CLASS instrument of the Chandrayaan 2 mission, within the framework of the PRADAN project, has yielded valuable insights into the X-ray Fluorescence (XRF) spectral data. The results of this analysis are presented below. The first step in the analysis involved converting channel numbers to energy values in kiloelectron volts (keV). The conversion formula used was:

$$\text{Energy (keV)} = (\text{Channel} * 13.5) / 1000$$

This conversion facilitated the interpretation of the spectral data in terms of energy levels, allowing for a more precise characterization of XRF signals.

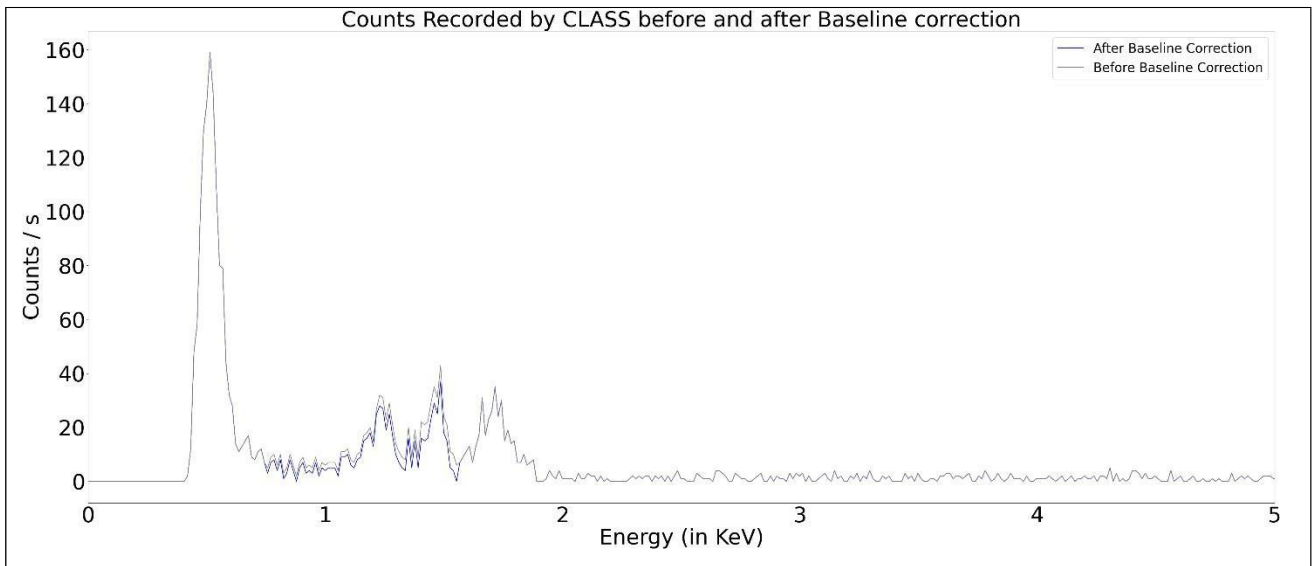


Figure19: The Energy vs Counts/s plot of the combined L1 FITS file of CLASS. The grey line depicts the plot before applying the baseline correction and the blue plot is that after the baseline correction.

Upon examination of individual 8-second integration files, it became evident that the data from a single file lacked sufficient information for the identification of XRF signals. To address this limitation, two L1 FITS files were selected and their corresponding channel and counts data were combined. This strategic data combination significantly improved the quality and statistical robustness of the analysis. The analysis revealed the presence of distinct XRF signals within the spectra (Figure 19). The identified energy peaks were as follows:

- 0.51 keV: This peak represents a significant signal in the spectral data corresponding to lighter elements like C, N or O.



- 1.23 keV: The appearance of the magnesium (Mg) XRF signal at 1.23 keV indicated the presence of this element in the sample material.
- 1.48 keV: The aluminium (Al) XRF signal at 1.48 keV was a clear indicator of aluminium's presence in the target material.
- 1.73 keV: The silicon (Si) XRF signal at 1.73 keV demonstrated the occurrence of silicon in the sample.

Each identified peak underwent Gaussian fitting, enabling the precise characterization of its properties. The Gaussian fitting process provided the following parameters for each peak:

1. Amplitude: The amplitude of the Gaussian peak represents the peak's intensity or signal strength.
2. Centroid (Mean): The centroid of the peak is the energy value at the peak's centre.
3. Standard Deviation (Width): The standard deviation characterizes the width of the peak, reflecting its breadth or narrowness.

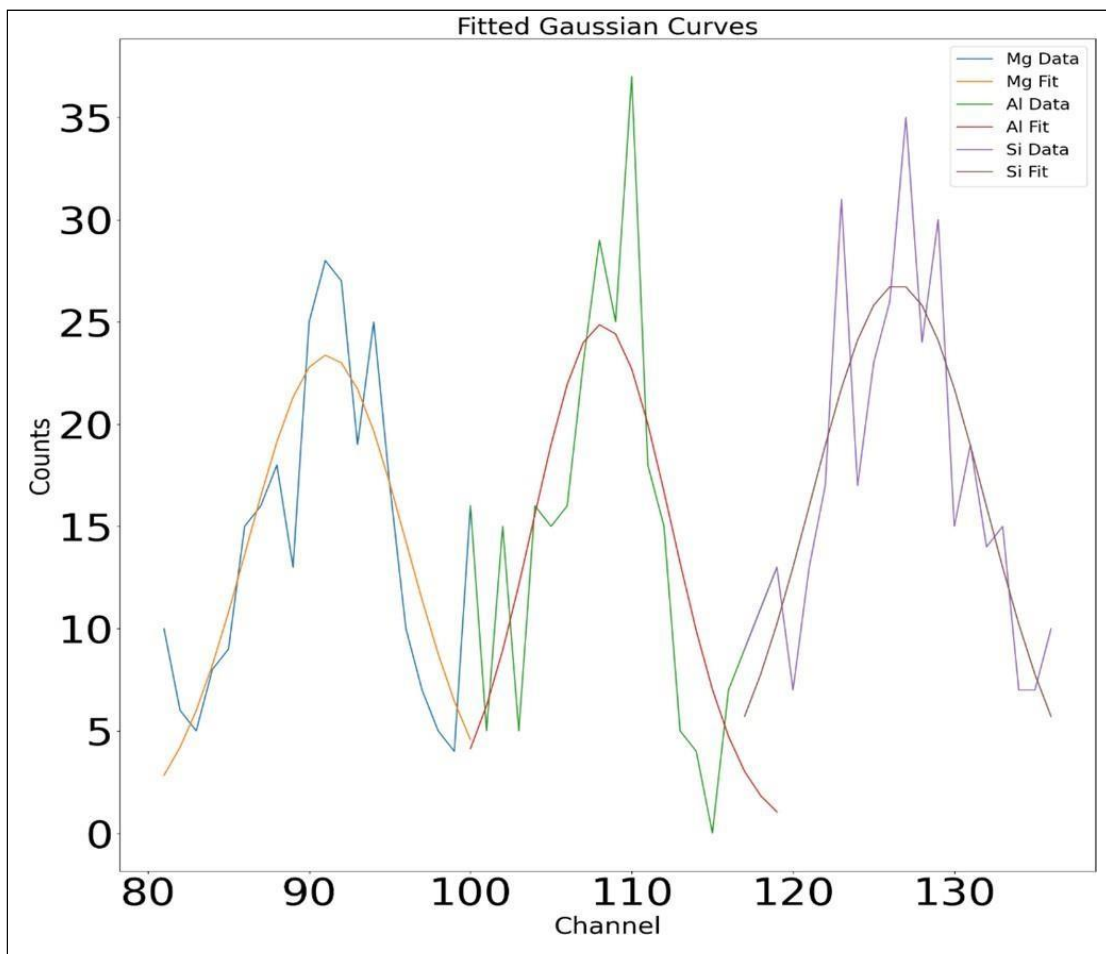


Figure20: Gaussian fitted curve for the XRF peaks detected in the combined L1 FITS CLASS files. The blue peak corresponds to Mg, green to Al and purple to that of Si. The orange curve fits the Mg peak, the red curve fits the AL peak whereas the brown fits the Si peak.

---

## CHAPTER 4: DISCUSSIONS

---

### 4.1 IBD ANALYSIS BASED ON M3 DATA

#### *4.1.1 Based on M3 Data*

The affirmation of mineral composition relies on the nuanced scrutiny of pixel spectra corresponding to clear-cut colours in the composite images. The specific spectral characteristics of minerals on the moon, such as pyroxene, spinel, anorthite, and olivine, are favourably situated within the Visible and Near-Infrared (VNIR) portion of the electromagnetic spectrum registered by M3. Spinel, for instance, manifests absorption at 2-micron, while ferroan anorthosite does so at 1.25-micron, olivine displays absorptions at 1-micron, and pyroxene exhibits its distinctive feature at both 1-micron and 2-micron<sup>[40]</sup>. To identify the presence of these minerals, the Integrated Band Depth (IBD) technique strategically focuses on the absorption features within these spectral regions, as previously highlighted in research<sup>[42][57]</sup>.

In the IBD colour composite illustrations depicting the surveyed region captured by M3, the wavelengths IBD1000, IBD2000, and IBD1250 were ascribed to the hues red, green, and blue, respectively (Figures 10 and 11). As a result, the resulting IBD colour amalgamation showcases spinel represented in green, pyroxene in yellow, olivine in red, and ferroan anorthosite in blue. It's crucial to take into account that the existence of Type A High-Ca pyroxene, known for its absorptions at 0.9 and 1.15 micron<sup>[40][58]</sup>, might appear as tones of magenta within the IBD colour composite. Hence, cautious consideration is required when interpreting these IBD colour blends, as they might inadvertently encompass biases triggered by topography<sup>[40][59]</sup>.

The IBD colour composite visuals (Figure 10) reveal a prevalence of the azure shade, linked to plagioclase in anorthosite, a primary rock type of the moon. Nevertheless, it's vital to acknowledge that the landscape also comprises altered plagioclase due to shock metamorphism, which might not be clearly emphasized in the produced colour composite pictures. Within this mainly blue area, isolated patches of pyroxene and spinel can be observed<sup>[40]</sup>.

To validate the presence of the previously mentioned minerals, an additional analysis entails inspecting the spectra obtained from pixels linked to different hues in the colour combinations (Figures 12 and 13). Spectra no.1 (blue) and 3 (green), characterized by absorption band centres at 1-micron and 2.1 micron, are representative of high-Ca pyroxene<sup>[40]</sup>. Spectra no.2 (orange), 4(red), and 5 (purple), with absorptions, centered at 0.95 micron and 1.95 micron, imply the existence of Low-Ca pyroxene<sup>[40]</sup>. Furthermore, the increased depth of the 2-micron absorption in Spectra no.3 suggests the involvement of another mineral phase, likely spinel. Spectra no.1, though similar to Spectra no.3, differs by having a shallower 2-micron absorption, indicating the absence of additional minerals. Conversely, Spectra no. 6 to 9, without a 1-micron characteristic and featuring conspicuous 2-micron absorptions, closely resemble spectra associated that of with spinel<sup>[40]</sup>.

The notion of band depth, assessed as the relative quantity of a substance, plays a pivotal role in deciphering the spectra. Band depth percentage is computed by deducting the reflectance value at the centre of the absorption band from the reflectance value within the continuum<sup>[60]</sup>, and then multiplying the outcome by 100<sup>[40]</sup>. In the scenario of a spectrum representing a combination of pyroxene and plagioclase, an abundance with less than 2% pyroxene there are no observable pyroxene absorption features<sup>[40][47]</sup>. In instances where pyroxene content ranges between 2-4%, the spectrum displays a 'w' pattern, exhibiting attributes of both pyroxene and plagioclase. Scenarios with an abundance exceeding 5 per cent pyroxene lead to characteristics primarily linked to pyroxene, potentially obscuring any 1.25-micron plagioclase feldspar feature, if it exists. Even with a 5% pyroxene component in the blend, the absorption related to pyroxene predominates, albeit with a subtle anorthositic absorption at 1.25-micron. As a result, in Spectra no.5, the pyroxene content is minimal, indicating a combination primarily composed of 96-98% plagioclase and 2-4% pyroxene<sup>[40]</sup>. Spectra no.4, though akin to Spectra no.5, signifies a higher pyroxene content. The nearly absent 1.3 micron feature in Spectra no.4 underscores a relative absorption intensity of 3.5%<sup>[40]</sup>.

The presence of Low-Ca pyroxene (Spectra no. 2, 4 and 5) in conjunction with feldspar resembles Pyroxferroite, a prevalent rock type in the lower crust of the Moon <sup>[40][61]</sup>. Pyroxferroite was among those 3 minerals that were identified on the lunar surface<sup>[86]</sup> during the Apollo 11 mission in 1969<sup>[62]</sup>. Conversely, the coexistence of High-Ca pyroxene (Spectra no. 1 and 3) with plagioclase suggests a gabbroic anorthosite lithology<sup>[40]</sup> consisting of minerals like apatite (fluorapatite to be more specific) again discovered during the Apollo

missions. Furthermore, the presence of spinel (Spectra no. 6-9) signifies the existence of a novel rock type in the region<sup>[40]</sup>, highlighting the diverse lithologies that necessitate an in-depth investigation of their respective spectra.

#### ***4.1.2 Based on IIRS Data***

The IBD colour composite images, which depict the study area as captured by IIRS, utilize specific wavelengths IBD1000, IBD2000, and IBD1250, corresponding to the colours red, green, and blue, respectively (Figure 17). As a result, the resulting IBD colour composite predominantly exhibits a colour that falls somewhere between pink and magenta.

Consequently, the IBD colour composite suggests the presence of elements that exhibit absorption patterns in both the red and blue bands (Table 3), meaning elements with absorptions around 1-micron and 1.25-micron. Additionally, specific regions exhibit a red and green hue, indicating the presence of elements with absorptions in the vicinity of the 1000 and 2-micron range.

These findings within the IBD results encompass the identification of specific minerals, such as Mg-Spinel, plagioclase feldspar, and pyroxenes, based on the distinctive positioning of their absorption bands. This positioning serves as a critical indicator of the presence of particular mineral species within the VNIR (Visible and Near-Infrared) region.

The spectral data acquired from the IIRS strip reveal notable characteristics that exhibit an absorption feature near 1-micron<sup>[88]</sup> while exhibiting a negligible absorption feature at 2-micron (the green region in the IBD map). The presence of Mg-Spinel is confirmed, as the 1-micron absorption feature is attributed to the existence of Fe<sup>2+</sup> ions in its tetrahedral crystallographic site<sup>[63]</sup>. Additionally, the broad absorption centred at 1.3-micron is a clear indication of plagioclase feldspar, a prevalent lunar mineral, with its distinct absorption feature attributed to the presence of Fe<sup>2+</sup> ions in its crystal structure<sup>[64][65]</sup>. It's worth noting that the presence of other mafic minerals, particularly pyroxenes, even in trace amounts, can obscure this diagnostic plagioclase feature<sup>[64]</sup>. Consequently, the spectral data likely signifies the presence of crystalline plagioclase feldspar. Moreover, a broad, faint feature at around 2-micron could suggest the presence of some mafic minerals, potentially Mg-Spinel. The spectra displaying dual absorption features in the ~1-micron and 2-micron regions in IIRS and M3, respectively, are diagnostic of pyroxenes. This phenomenon arises from electronic

transitions involving Fe<sup>2+</sup> ions within their crystallographic sites, with the band positions shifting as a function of Ca content<sup>[66]</sup>.

This IBD map represents initial findings related to mineral detection using IIRS data strips obtained from ISRO's recent Chandrayaan2 mission. Upon comparison with Ch-1 M3 [Figure 10], the spectra exhibit a noteworthy degree of similarity. Despite variations in observation geometry, spatial resolution, and wavelength resolution, the derived reflectance spectra closely align in their spectral characteristics. A comprehensive and meticulous analysis promises to yield a more profound understanding. Further data processing steps, including thermal removal, normalization to standard geometry, and ground-truth corrections, are expected to enhance the quality of results due to the IIRS sensor's superior spectral resolution capabilities.

## **4.2 Modified Gaussian Model (MGM)**

### ***4.2.1 Based on M3 Analysis***

The MGM (Modified Gaussian Model) technique plays a role in providing a more intricate comprehension of the mineral composition encompassed within the deconvoluted spectral bands. In the case of Spectra no.1 and Spectra no.3, the band centres derived from the MGM (Table 4) indicate a blend of anorthitic plagioclase<sup>[40]</sup>, olivine, spinel and pyroxene.

Specifically, BC1 (band centre 1) for Spectra no.1 and 3 is detected just past 0.94-micron, signalling the presence of high-Ca pyroxene. The corresponding 2-micron band centre (BC4) is located at approximately 2.1-micron for both Spectra no.1 and Spectra no.3. These two spectra also exhibit absorption corresponding to plagioclase at 1.21-micron, referred to as BC2. Additionally, the spectrum of Mg-spinel displays a noticeable absorption peak centred at under 1.9-micron. BC3 for Spectra no.1 and 2 can be linked to Mg-spinel.

Spectra no.2, 4 and 5, which exhibit two absorption bands at 2-micron and two at 1-micron, indicate the presence of two types of pyroxenes. B2C and B4C, at 1.2-micron and 2.1 micron, respectively, indicate High-Ca pyroxene<sup>[40]</sup> whereas B1C and B3C, at 0.9-micron and 1.8 micron, respectively, point toward Low-Ca pyroxene<sup>[40]</sup>. It's crucial to acknowledge that the band centred at 0.8 micron (B0C) represents a sensor-induced error (Li et al., 2018). Notably, absorption bands corresponding to Spinel were not observed in Spectra no. 2, 4 and 5.

The presence of olivine in the study area cannot be entirely ruled out, as it is a common constituent in the FHT (Ferroan Anorthosite Highlands Terrain) lithologies. Deconvolution of laboratory olivine spectra typically reveals three absorption bands centred around 1-micron, specifically at 0.85-micron, 1.05-micron, and 1.25-micron<sup>[40]</sup>. However, lacking an 0.83 micron band in the deconvolved M3 spectra of spectrum 4 does not conclusively negate the presence of olivine (though it is present in spectra 2 and 5). Notably, spectral analysis of M3-derived spectra from certain central peaks known for their high olivine content, did not consistently exhibit absorptions at 0.83-micron<sup>[40]</sup>. Consequently, the absence of an 0.83-micron band in deconvolved M3 spectra does not necessarily preclude the presence of olivine. Nevertheless, olivine has not been contemplated as the paramount mineral in the composition of the mare region of study.

Lastly, Type A High-Ca pyroxene, characterised by absorption at 1.15-micron, could affect the deconvolved band at 1.25-micron. However, MGM deconvolution results did not yield any absorption band explicitly centred at 1.15-micron. Additionally, Type A pyroxene dearths a noteworthy 2-micron absorption feature. Therefore, attributing the 1.25-micron absorption to Type A pyroxene raises inconsistencies, as it would necessitate a corresponding absorption band centred around 2-micron<sup>[40]</sup>, which was not observed. In light of these findings, it becomes evident that the region comprises a diverse assortment of rocks, featuring pyroxenes, anorthitic plagioclase, and spinel, among other constituents.

### **4.3 Mg-Spinel Detection**

The presence of Mg-spinel and its connection to magnesian suite rocks requires thorough analysis, as it holds potential insights into the evolution of the lunar crust. Mg-spinel was initially identified through M3 data analysis<sup>[67][68]</sup>. Subsequent research revealed its presence on both the near side and far side of the Moon. This discovery led to the identification of a new lunar rock type known as "pink spinel anorthosite" (PSA)<sup>[40]</sup>, characterized by its abundance of Mg-spinel and a scarcity (less than 5%) of mafic minerals such as olivine and pyroxene<sup>[68][69][70]</sup>.

Various theories have been proposed to explain the origin and distribution of Mg-spinel. These include (i) its formation through interactions between lunar crustal magma and surrounding rocks, involving processes like assimilation and fractional crystallization<sup>[71][72]</sup>,

(ii) production during the formation of lunar impact basins<sup>[73]</sup>, (iii) origin through impact melt processes<sup>[74]</sup>, and (iv) possible association with projectile remnants from meteorite impacts<sup>[75]</sup>. Typically, Mg-spinel has been found in crater rims, walls, central peaks, and inner rings of larger impact basins<sup>[70]</sup>, suggesting that the spinel-rich material was initially deep-seated and brought to the surface during impact events, possibly creating a mixture of anorthositic crust and mantle material<sup>[40][67][68]</sup>.

The lunar mantle layer, primarily composed of pyroxene and olivine, is the source of basaltic magmatism<sup>[40]</sup> on the Moon<sup>[76][77][78][79][80]</sup>. The presence of spinel alongside pyroxene in this examination proposes a potential connection between these minerals and similar basalts.

Although there are no spectral imprints of basalt in the study area, any existing basalt would likely be a subsurface intrusion younger than the Korolev impact<sup>[40]</sup>. However, in a three-component phase diagram involving quartz, pyroxene, and olivine, the chances of spinel and pyroxene co-crystallizing are extremely low. It is more probable that spinel and olivine would form together, making it a rare occurrence for spinel and pyroxene to be co-crystallising<sup>[40]</sup>  
<sup>[81][82][83]</sup>

. Nevertheless, mantle basalts could undergo fractional crystallization as they ascend toward the lunar crust, resulting in the formation of spinel-rich lithologies at shallower depths.

Furthermore, it was proposed that PSA may form directly during the cooling of superliquidus melts with an anorthite-rich composition generated by impact events<sup>[40][74]</sup>. Based on Spinel's experimentally observed temperature stability, it has been concluded that speedy crystallization of impact melts with an anorthosite-rich composition is the most likely procedure for spinel formation near the lunar surface<sup>[40]</sup>. This theory also dismisses the notion that spinel-bearing lithology originated from the uplift of deep-seated material to the lunar surface<sup>[40][74]</sup>. In light of these considerations, the study sought to investigate the morphological associations of spinel with other minerals to gain insights into their origins.

## **4.4 Comparing with CLASS Abundance file**

### ***4.1 Lunar Elemental Analysis Methods***

In the past, efforts have been made to create global maps of refractory elements using various methods. Some studies utilised direct approaches involving gamma-ray measurements, others employed indirect methods using UV-Vis-IR (Ultraviolet-Visible-Infrared) measurements. A

direct approach for estimating elemental abundances on the lunar surface is X-ray fluorescence spectroscopy, where the intensities of XRF lines<sup>[84]</sup> at specific energy levels are directly proportionate to the element's abundance. This method relies on physical models rather than empirical relationships<sup>[85]</sup>.

In contrast, UV-Vis-IR measurements derive quantitative abundance estimates<sup>[84]</sup> through parametric dependencies of spectral parameters based on empirical relations, often using returned lunar samples or LP-GRS (Lunar Prospector Gamma-Ray Spectrometer) global elemental maps as references. The elements most commonly mapped are iron (Fe) and titanium (Ti) due to their distinct signatures in UV-Vis-IR and gamma wavelengths<sup>[84]</sup>.

However, mapping magnesium (Mg), aluminium (Al), and silicon (Si) has been more puzzling, even with gamma-ray spectroscopy, mainly because of lower spectral resolution and background noise in the detectors. Additionally, a significant discrepancy in spatial scales between UV-Vis-IR and gamma-ray measurements limits explicit evaluations of the outcomes obtained from these methods.

X-ray fluorescence spectroscopy operates by identifying characteristic photons emitted by atoms within a material when excited by an external X-ray photon source<sup>[84]</sup>. The intensity of these photon lines is directly related to the number of atoms, or in other words, the abundance of the element emitting them. For major lunar elements, K- $\alpha$  X-ray fluorescence energies<sup>[84]</sup> are sufficiently distinct, allowing their measurement with moderate-resolution X-ray spectrometers. Early measurements, like those on Luna 10-12, Apollo 15, and Apollo 16 missions, relied on gas-based counters. Although they covered a huge zone, they required spectral resolution and the capability to measure low-energy lines from low atomic number elements<sup>[84]</sup>. Semiconductor X-ray detectors<sup>[84]</sup> were initially deployed on SMART-1 and successively on missions like Kaguya, Chang'e-1 and 2<sup>[84]</sup>, and Chandrayaan-1. However, some of these detectors faced challenges such as radiation impairment, which made resolving the low-energy lines of elements like Mg, Al, and Si difficult.

An experiment called D-CIXS on SMART-1 validated the potential of Si-based detectors for lunar elemental reports<sup>[84]</sup> but stood from radiation impairment. Kaguya-XRS, equipped with an array of X-ray CCDs<sup>[84]</sup>, also faced radiation impairment issues that prohibited beneficial measurements. Chang'e-1 and 2 carried Si-PIN detectors with poor spectral resolution, and their operational periods coincided with very low solar activity, limiting the data obtained. Abundances of elements like Mg, Al, Si, Ca, Ti, and Fe were successfully derived from the



Chang'e-2 X-ray spectrometer for a region in Oceanus Procellarum. The Chandrayaan-1 mission featured C1XS, which had excellent spectral resolution and a low-energy threshold, aiming to create elemental maps at a 25 km scale. Unfortunately, due to awfully gloomy solar activity and a short nine-month mission duration, only a few localised regions of the Moon were thoroughly mapped.

In planetary remote sensing using X-ray emission, solar X-rays play a significant role. The solar X-ray spectrum is extremely flexible, especially during solar flares<sup>[84]</sup>. Therefore, a simultaneous measurement of the solar spectrum is crucial for accurately determining elemental abundances. All the researches mentioned above included simultaneous measurements of the solar spectrum using Si-PIN detectors<sup>[84]</sup>. The operation of these solar monitors is crucial for precise elemental abundance determination.

CLASS features sixteen swept charge devices (SCDs)<sup>[84]</sup>, similar to those in D-CIXS and C1XS but with design improvements to achieve better spatial and spectral resolution. It is accompanied by a Solar X-ray Monitor (XSM) with a Silicon Drift Detector (SDD), which measures the solar spectrum simultaneously with the lunar X-ray measurements<sup>[84]</sup>.

The CLASS instrument has conducted precise measurements of the lunar X-ray fluorescence (XRF)<sup>[89]</sup> spectrum in various regions, offering elevated spectral resolution that effectively recognizes all major elements. During solar flares, solar X-rays interact with the Moon's surface, causing excited atoms to emit fluorescent X-rays. CLASS is specifically designed to detect this X-ray emission within the energy range of 0.8 to 15 keV. To gain a comprehensive understanding of the X-ray spectrum produced by solar flares, which triggers the generation of fluorescent X-rays, Chandrayaan-2 carries a complementary payload, the X-ray Solar Monitor. This monitor observes the Sun simultaneously to measure the spectrum of solar flare X-rays.

The output from the CLASS instrument provides time-tagged events for each Swept Charge Device (SCD), which are grouped in time intervals to create the X-ray spectra. These spectra are analysed by fitting the spectral lines using a Gaussian function and the 'mpfit' routine in IDL (Interactive Data Language). Calibration parameters are then derived for all 16 SCDs.

#### ***4.4.2 CLASS Data***

The following are the features of the downloaded dataset  
ch2\_cla\_11\_20220418T043313070\_20220418T043321070 and  
ch2\_cla\_11\_20220418T043321070\_20220418T043329070;

(1) Each Level 1 (L1) FITS file comprises 2048 channels with a gain of 13.5 eV per channel, (2) The raw spectra have been adjusted to the 0th channel, meaning there is no offset, (3) In the analysis of lunar spectra, channels falling within the range of 37-800 (0.5-10 keV) are considered, while channels above 1112 (approximately 15 keV) and below 37 (0.5 keV) are disregarded, and (4) Lone data points or spikes in any channel should not be included in the analysis.

The provided figure serves as a graphical representation of the data obtained from the CLASS instrument. This data illustrates the relationship between the energy levels or channels and the corresponding counts recorded in the combined Level 1 (L1) FITS files, which have been meticulously collected by the CLASS instrument during its lunar observations. In essence, this plot visually encapsulates the wealth of information captured by the instrument, enabling a detailed examination of the X-ray fluorescence (XRF) signals emanating from the lunar surface.

Within the plot, distinct peaks become immediately evident. These peaks signify the presence of specific XRF signals, each associated with a particular element. It is this discerning capability of CLASS that allows us to pinpoint the energy levels at which these peaks occur, which in turn provides a direct link to the identification of the chemical elements responsible for generating these XRF signals. In this context, the figure reveals k- $\alpha$  peaks at energy levels of 0.51 keV, 1.23 keV, 1.48 keV, and 1.73 keV. These energy levels correspond to the characteristic XRF signals of elemental oxygen (O), magnesium (Mg), aluminium (Al), and silicon (Si), respectively. The precision of this identification is paramount in elemental analysis and contributes significantly to our understanding of the composition of lunar materials.

Gaussian fitting (shown in Figure), as employed in this analysis, plays a pivotal role in the field of mineral and elemental identification. It offers a powerful analytical approach that enables both quantitative and qualitative insights into the spectral data. Further analysis with

CLASS data can be carried out based on the Gaussian fitting of these peaks. Through the application of Gaussian fitting, the peaks' parameters are characterised, allowing a comprehensive examination of the spectral features. It provides the capability for deconvolution, effectively separating overlapping peaks, and thus facilitating the clear identification of multiple elements. Additionally, it contributes to noise reduction. Ultimately, Gaussian fitting empowers scientists to make detailed comparisons between different spectral features and, most importantly, to confidently identify the elemental composition of the samples under examination.

The elemental maps obtained from PRADAN are a valuable resource, encompassing five different elemental maps for sodium (Na), magnesium (Mg), aluminium (Al), silicon (Si), and iron (Fe). These maps exhibit gradients, which provide insights into the spatial distribution of these elements across the lunar surface. Notably, the Mare Tranquillitatis region is highlighted in the maps, indicating specific areas of interest for further analysis.

The elemental maps reveal distinctive patterns of elemental abundance in the Mare Tranquillitatis region. Notably, sodium (Na) is present at low levels, magnesium (Mg) at moderate levels, and aluminium (Al), silicon (Si), and iron (Fe) at high levels. The gradients for aluminium (Al) and silicon (Si) have a notably higher low value, starting from around 5-6, while other elements exhibit much lower values for the least gradient, starting from around 1. These elemental distribution patterns are significant for understanding the composition and geological characteristics of the lunar surface in the Mare Tranquillitatis region<sup>[86]</sup>.

---

## CHAPTER 5: SUMMARY AND CONCLUSION

---

In conclusion, the comprehensive study presented in these four chapters provides invaluable insights into the mineralogical and elemental composition of the lunar surface, particularly in the intriguing Mare Tranquillitatis region<sup>[86]</sup>. By employing a synergistic approach, utilising data from M3, IIRS, and CLASS, researchers have pieced together a multi-dimensional understanding of the complex lunar geology.

Initially, the foundation was laid by introducing the mission's objectives, scientific instruments, and data acquisition methods setting the stage for a detailed examination of lunar composition, and exploring the role of orbital remote sensing techniques in advancing our knowledge of celestial bodies. The sophistication and precision of the instruments, including M3, IIRS, and CLASS were highlighted as integral to the success of the mission.

Next, through the Integrated Band Depth (IBD) technique<sup>[87]</sup>, the M3 instrument provided rich insights into the presence of key lunar minerals, such as anorthite, pyroxene, olivine, and spinel. The use of colour composite images, created from specific absorption features within the Visible and Near-Infrared (VNIR) region<sup>[40]</sup>, enabled the identification of these minerals, with olivine appearing in red, spinel in green, ferroan anorthosite in blue, and pyroxene in yellow. The significance of this technique lies in its ability to discern mineral compositions and the potential for novel discoveries, such as the existence of Type A High-Ca pyroxene<sup>[40]</sup>, which may manifest as shades of magenta. It underscores the need for careful interpretation of these IBD colour composites, as topographic influences can introduce biases.

The analysis is further enriched by the examination of spectra from different colour composites, shedding light on the subtle variations in mineral composition. These spectra reveal the presence of High-Ca and Low-Ca pyroxenes, as well as Mg-Spinel, which opens the door to exciting geological inferences. The identification of specific mineral phases, such as Pyroxferroite and apatite, and their coexistence with High-Ca pyroxene suggest gabbroic anorthosite lithologies. Additionally, the presence of spinel hints at novel rock types within the study area, calling for further detailed investigation.

Later, the study expands upon these findings by introducing data obtained from IIRS. The IBD technique is again applied, this time revealing colour composites dominated by magenta shades. These colour composites are instrumental in the identification of Mg-Spinel, plagioclase feldspar, and pyroxenes. The unique capability of the IIRS data to detect these materials further enhances the overall understanding of lunar mineralogy.

The comparability of results from M3 and IIRS reinforces the robustness of the findings. The presence of Mg-Spinel<sup>[88]</sup>, the most exciting discovery in the IIRS data, not only corroborates the earlier Mg-Spinel identification from M3 but also underscores the need for further examination of lunar basalts. The presence of High-Ca pyroxenes points toward gabbroic anorthosite lithologies, likely the apatites. As the study area presents a diverse assortment of minerals, including spinel, anorthitic plagioclase, and pyroxenes, a deeper understanding of their origins and associations is warranted. Collectively, the data from M3 and IIRS provide a consistent picture of the lunar surface's mineralogical composition.

Following that, the study delved into the elemental analysis, primarily through the data gathered by CLASS. This instrument utilises X-ray fluorescence<sup>[89]</sup> (XRF) spectroscopy, allowing researchers to examine the spectral signatures of elements on the lunar surface. The elemental analysis complements the mineralogical insights provided by M3 and IIRS, offering a multi-dimensional view of lunar composition.

The CLASS data presents k- $\alpha$  XRF peaks indicative of specific elements, such as oxygen (O), magnesium (Mg), aluminium (Al), and silicon (Si)<sup>[90]</sup>. The precision of the instrument enabled researchers to determine the energy levels at which these peaks occur, facilitating the identification of these chemical elements. Utilising Gaussian fitting, the spectral data can be meticulously analysed ahead, allowing for accurate quantification of elemental abundances and noise reduction. Moreover, Gaussian fitting permits the deconvolution of overlapping peaks, enhancing the identification of multiple elements within complex spectra. This in-depth elemental analysis will be crucial in understanding the composition of lunar materials.

Complementing the XRF data from CLASS, the elemental maps reveal the spatial distribution of sodium (Na), magnesium (Mg), aluminium (Al), silicon (Si), and iron (Fe). Notably, the Mare Tranquillitatis region stands out in these maps, offering areas of significant interest for further exploration. The elemental distribution patterns provide valuable insights

into the geological and compositional aspects of the lunar surface, further enriching our understanding.

The integrated approach of this study, drawing from the capabilities of M3, IIRS, and CLASS instruments, has significantly advanced our understanding of lunar composition. The mineralogical insights, the identification of novel rock types, and the comprehensive elemental analysis all contribute to a multi-dimensional understanding of the Mare Tranquillitatis region. The consistent findings and corroborations across different data sources validate the scientific rigour and reliability of the study.

These findings have far-reaching implications for lunar geology and planetary science. The identification of Mg-Spinel<sup>[40]</sup> and its association with impact events opens new avenues for exploring lunar geological history. The presence of High-Ca pyroxenes and their connection to gabbroic anorthosite lithologies offer further insights into the lunar crust's complexity and evolution. The elemental analysis, through XRF data, contributes to our understanding of the Moon's composition, including the distribution of essential elements like oxygen, magnesium, aluminium, silicon, and iron.

This collaborative and comprehensive study serves as a testament to the remarkable capabilities of lunar remote sensing instruments and paves the way for future missions and investigations. As humanity continues its exploration of celestial bodies, the knowledge gained from the Chandrayaan missions plays a pivotal role in unravelling the mysteries of the cosmos.

## REFERENCES:

- 
- <sup>1</sup> "Mare | lunar feature". Encyclopedia Britannica. Retrieved (2021)
- <sup>2</sup> Starr, Michelle, *The Moon Is Lopsided, And New Research Could Finally Explain Why*, ScienceAlert. Retrieved (2021)
- <sup>3</sup> Jolliff, Bradley L.; Gillis, Jeffrey J.; Haskin, Larry A.; Korotev, Randy L.; Wieczorek, Mark A., *Major lunar crustal terranes: Surface expressions and crust-mantle origins*. Journal of Geophysical Research: Planets. (2000)
- <sup>4</sup> "APOLLO 16". history.nasa.gov. Retrieved 2021-02-22
- <sup>5</sup> Taylor, G. Jeffrey. "PSRD: New ideas on the nature of the Moon". www.psrh.hawaii.edu. Retrieved 2021-02-22. (2000)
- <sup>6</sup> Hawke, B.R., Spudis, P.D., Geochemical anomalies on the eastern limb and farside of the moon. Conference on the Lunar Highlands Crust, 467–481. (1980)
- <sup>7</sup> Hawke, B.R., Spudis, P.D., Clarke, P.E., The Origin of selected lunar geochemical anomalies: Implications for early volcanism and the formation of light plains. Earth Moon Planet. 32, 257–273. (1985)
- <sup>8</sup> Genda, H. Giant Impact Hypothesis. In: White, W. (eds) Encyclopedia of Geochemistry. Encyclopedia of Earth Sciences Series. Springer, Cham. (2017)
- <sup>9</sup> Boss AP The origin of the moon. Science 231:341–345 (1986)
- <sup>10</sup> Jolliff, B. L., et al. Major lunar crustal terranes: Surface expressions and crust-mantle origins. Journal of Geophysical Research: Planets (2000)
- <sup>11</sup> H. ST.C. O'NEILL: The origin of the Moon and the early history of the Earth-A chemical model. Part 1: The Moon (1991)
- <sup>12</sup> J. N. Goswami and M. Annadurai Chandrayaan-1: India's first planetary science mission to the moon (2010)
- <sup>13</sup> Pieters, C. M., et al.: Character and Spatial Distribution of OH/H<sub>2</sub>O on the Surface of the Moon Seen by M3 on Chandrayaan-1. (2009)
- <sup>14</sup> Sunshine, J. M., et al.: Temporal and Spatial Variability of Lunar Hydration As Observed by the Deep Impact Spacecraft. Science (2009)
- <sup>15</sup> Venkatesan Sundararajan: Overview and Technical Architecture of India's Chandrayaan-2 Mission to the Moon (2018)
- <sup>16</sup> [www.isro.gov.in](http://www.isro.gov.in)
- <sup>17</sup> Green, R. O. et al.: Calibration, shipment and initial spacecraft integration of the Moon Mineralogy Mapper (M3) imaging spectrometer for the Chandrayaan-1 mission. (2008)
- <sup>18</sup> Carle M. Pieters: The Moon Mineralogy Mapper (M3) on Chandrayaan-1 (2008)
- <sup>19</sup> Pieters, C. M.; The Moon as a spectral calibration standard enabled by lunar samples: the Clementine example. (1999)

- 
- <sup>20</sup> Athiray P. S., S. Narendranath, P.S.M.G., 2014. C1xs results—first measurement of enhanced sodium on the lunar surface. (2014)
- <sup>21</sup> Netra S Pillai, S. Narendranath, K. Vadodariya, Srikar P Tadepalli, Radhakrishna V, Anurag Tyagi, Reena Yadav, Brajpal Singh, Vaishali Sharan, P. S. Athiray, P. Sree Kumar, K. Sankarasubramanian, Megha Bhatt, Amit Basu Sarbadhikari, N. P. S. Mithun, Santosh Vadawale: Chandrayaan-2 Large Area Soft X-ray Spectrometer (CLASS): Calibration, In-flight performance and first results (2021).
- <sup>22</sup> Nittler, L. R., et al.: Element abundance analyses of closed-basin impact melt pools on the Moon using Chandrayaan-2 X-ray Spectrometer data. (2021)
- <sup>23</sup> Klima, R. L., et al.: Imaging Infrared Spectrometer (IIRS) on Chandrayaan-2 for Study of Minerals, Water Molecules and Hydroxyl on the Moon. (2019)
- <sup>24</sup> Putrevu et al. Chandrayaan-2 Dual-Frequency SAR: Further Investigation Into Lunar Water and Regolith (2015)
- <sup>25</sup> Byrne, C. J., Ostrach, L. R., & Whitten, J. L.: The geologic history (2014)
- <sup>26</sup> Bhatt et al.: Compositional mapping and the evolutionary history of Mare Tranquillitatis (2020).
- <sup>27</sup> Bhatt et al.: Timing and Origin of Compressional Tectonism in Mare Tranquillitatis (2020)
- <sup>28</sup> Bhatt et al.: Mineralogical and Geomorphological Mapping of western central part of Mare Tranquillitatis using Hyperspectral Imager onboard Chandrayaan-1 (2018)
- <sup>29</sup> Spudis, P. D.: Mare Tranquillitatis Region Characteristics and Significance: (1993)
- <sup>30</sup> Jolliff, B. L., et al.: Geochemical Characteristics of Mare Tranquillitatis (2000)
- <sup>31</sup> Pieters, C. M.: Character and Spatial Distribution of OH/H<sub>2</sub>O on the Surface of the Moon Seen by M3 on Chandrayaan-1 (2008)
- <sup>32</sup> Sunshine, J. M., et al.: Remote sensing of H<sub>2</sub>O and OH on the Moon with the Moon Mineralogy Mapper (M3) (2009)
- <sup>33</sup> Parthasarathy, G., et al.: Chandrayaan-2 Large Area Soft X-ray Spectrometer (CLASS): Design and Performance (2020)
- <sup>33</sup> Taylor, S. R., & McLennan, S. M.: Planetary Crusts: Their Composition, Origin, and Evolution (Chapter 4) (2009).
- <sup>34</sup> Y., Jiang & T., Kang & Y., Liao & M., Elardo & Q., Zong & J., Wang & C., Nie & Y., Li & J., Yin & F., Huang & B, Hsu.: Fe and Mg Isotope compositions Indicate a Hybrid Mantle Source for Young Chang'E 5 Mare Basalts (2023)
- <sup>35</sup> Xuejin, Lu & Cao, Haijun & Ling, Zongcheng & Fu, Xiaohui & Qiao, Le & Chen, Jian. . Geomorphology, Mineralogy, and Geochronology of Mare Basalts and Non-Mare Materials around the Lunar Crisium Basin (2021)
- <sup>36</sup> Dygert, Nick & Liang, Yongtu & Hess, P.: The Effect of Melt TiO<sub>2</sub> on Fe-Ti Oxide-Picritic Basalt HFSE Partitioning: Parameterized Models, Lunar Applications (2012)



- 
- <sup>37</sup> Paul D. Spudis: Volcanism on the Moon (2015)
- <sup>38</sup> Papike, James & Simon, Steven & Shearer, Charles.: The effects of contrasting Ti and Al activities on Mn/Fe systematics in pyroxene from lunar mare basalts (2019).
- <sup>39</sup> Joshua R. Evans; QScout: A QGIS plugin tool suite for georeferencing and analysis of field-scouted and remote sensing data (2021)
- <sup>40</sup> N. Chaudhuri, K.N. Kusuma, S. Aravind Bharathvaj.: Understanding the mineralogy of a compositional anomaly north of the Korolev basin using Moon Mineralogy Mapper", *Advances in Space Research* (2022)
- <sup>41</sup> Boardman, J.W., Kruse, F.A.; Automated spectral analysis: a geological example using AVIRIS data, north Grapevine Mountains, Nevada: Proceedings of the Thematic Conference on Geologic Remote Sensing (1994)
- <sup>42</sup> Mustard, J.F., Pieters, C.M., Isaacson, P.J., Head, J.W., Besse, S., Clark, R.N., Klima, R.L., Petro, N.E., Staid, M.I., Sunshine, J.M., Runyon, C.J., Tompkins, S.; Compositional diversity and geologic insights of the Aristarchus crater from Moon Mineralogy Mapper data (2011)
- <sup>43</sup> Besse, S., Sunshine, J.M., Staid, M.I., Petro, N.E., Boardman, J.W., Green, R.O., Head, J.W., Isaacson, P.J., Mustard, J.F., Pieters, C.M.; Compositional variability of the Marius Hills volcanic complex from the Moon Mineralogy Mapper (M3) (2011)
- <sup>44</sup> Pieters, C.M., Hanna, K.D., Cheek, L., Dhingra, D., Prissel, T., Jackson, C., Moriarty, D., Parman, S., Taylor, L.A.; The distribution of Mg-spinel across the Moon and constraints on crustal origin (2014)
- <sup>45</sup> Harald van der Werff, Freek van der Meer & Steven de Jong: Exercise: Continuum removal and spectral feature finding (2011)
- <sup>46</sup> Cheek, L.C., Donaldson Hanna, K.L., Pieters, C.M., Head, J.W., Whitten, J.L.; The distribution and purity of anorthosite across the Orientale basin: new perspectives from Moon Mineralogy Mapper data (2013)
- <sup>47</sup> Staid, M.I., Pieters, C.M., Besse, S., Boardman, J., Dhingra, D., Green, R., Head, J.W., Isaacson, P., Klima, R., Kramer, G., Mustard, J.M., Runyon, C., Sunshine, J., Taylor, L.A.; The mineralogy of late stage lunar volcanism as observed by the Moon Mineralogy Mapper on Chandrayaan-1(2011)
- <sup>48</sup> Crowley, J.K., Brickey, D.W., Rowan, L.C.; Airborne imaging spectrometer data of the Ruby Mountains, Montana: mineral discrimination using relative absorption band-depth images (1989)
- <sup>49</sup> Sunshine, J.M., Pieters, C.M.; Estimating modal abundances from the spectra of natural and laboratory pyroxene mixtures using the modified Gaussian model (1993)
- <sup>50</sup> Sunshine, J.M., Pieters, C.M.; Determining the composition of olivine from reflectance spectroscopy (1998)
- <sup>51</sup> Sunshine, J.M., Pieters, C.M., Pratt, S.F.; Deconvolution of mineral absorption bands: an improved approach (1990)
- <sup>52</sup> Isaacson, P.J., Pieters, C.M., Besse, S., Clark, R.N., Head, J.W., Klima, R.L., Mustard, J.F., Petro, N.E., Staid, M.I., Sunshine, J.M., Taylor, L.A., Thaisen, K.G., Tompkins, S.; Remote compositional analysis of lunar olivine-rich lithologies with Moon Mineralogy Mapper (M3) spectra (2011)
- <sup>53</sup> Crowley, J.K., Brickey, D.W., Rowan, L.C., 1989. Airborne imaging spectrometer data of the Ruby Mountains, Montana: mineral discrimination using relative absorption band-depth images

---

<sup>54</sup> new.isro.gov.in

<sup>55</sup> Kneen, M. A.; Annegarn, H. J. Algorithm: Fitting XRF, SEM and PIXE X-Ray Spectra Backgrounds (1996)

<sup>56</sup> Liland KH, Almøy T, Mevik B: Optimal Choice of Baseline Correction for Multivariate Calibration of Spectra (2010)

<sup>57</sup> Besse, S., Sunshine, J.M., Staid, M.I., Petro, N.E., Boardman, J.W., Green, R.O., Head, J.W., Isaacson, P.J., Mustard, J.F., Pieters, C.M: *Compositional variability of the Marius Hills volcanic complex from the Moon Mineralogy Mapper (M3)*. (2011)

<sup>58</sup> Cloutis, E.A., Gaffey, M.J.: *Pyroxene spectroscopy revisited: Spectral-compositional correlations and relationship to geothermometry*. (1991)

<sup>59</sup> Grumpe, A, Brinkmeier, F, Wohler, C: *Analysis of Topographic Effects Observed in Spectral Features Extracted from Chandrayaan-1 M3 Imagery* (2011)

<sup>60</sup> Clark, R.N., Roush, T.L.: *Reflectance spectroscopy: quantitative analysis techniques for remote sensing applications* (1984)

<sup>61</sup> Pieters, C.M., Tompkins, S., Head, J.W., Jolliff, B., Hess, P.C., 1997. Mineralogy of the mafic anomaly in South-Pole Aitken Basin: implications for the excavation of the lunar mantle. *Geophys. Res. Lett.* 24, 1903–1906

<sup>62</sup> Chao, E. C. T.; et al.: *Pyroxferrite, a new calcium-bearing iron silicate from Tranquillity Base*. (1970)

<sup>63</sup> Cloutis, E. A. et al.: *Spectral reflectance properties of ureilites* (2004)

<sup>64</sup> Pieters C. M.: *Strength of mineral absorption features in the transmitted component of near-infrared reflected light* (1983)

<sup>65</sup> Adams J. B., Hörz F., and Gibbons R. V.: *Effects of shock-loading on the reflectance spectra of plagioclase, pyroxene and glass* (1979)

<sup>66</sup> Adams J. B., Pieters C., and McCord T. B.: *Orange glass: Evidence for regional deposits of pyroclastic origin on the Moon* (1974)

<sup>67</sup> Dhingra, D., Pieters, C.M., Boardman, J.W., Head, J.W., Isaacson, P.J., Taylor, L.A.: *Compositional diversity at Theophilus Crater: Understanding the geological context of Mg-spinel bearing central peaks*. (2011)

<sup>68</sup> Pieters, C.M., Hanna, K.D., Cheek, L., Dhingra, D., Prissel, T., Jackson, C., Moriarty, D., Parman, S., Taylor, L.A.: *The distribution of Mg-spinel across the Moon and constraints on crustal origin* (2014)

<sup>69</sup> Jackson, C.R.M., Cheek, L.C., Parman, S.W., Cooper, R.F., Pieters, C. M.: *Compositional constraints on lunar spinel anorthosite: Synthesis of spinel with variable iron content* (2012)

<sup>70</sup> Prissel, T.C., Parman, S.W., Jackson, C.R.M., Rutherford, M.J., Hess, P. C., Head, J.W., Cheek, L., Dhingra, D., Pieters, C.M.: *Pink Moon: The petrogenesis of pink spinel anorthosites and implications concerning Mg-suite magmatism* (2014)

<sup>71</sup> Gross, J., Treiman, A.H.: *Unique spinel-rich lithology in lunar meteorite ALHA 81005: origin and possible connection to M3 observations of the farside highlands* (2011)

- 
- <sup>72</sup> Prissel, T.C., Parman, S.W., Jaackson, C.R.M., Dhingra, D, Ganskow, G, Cheek, L.C., Rutherford, M.J., Hess, P, Pieters, C.M.: *Melt-wallrock reactions on the Moon: Experimental constraints on the formation of newly discovered Mg-spinel anorthosites* (2012)
- <sup>73</sup> Vaughan, W.M., Head, J.W., Wilson, L., Hess, P.C.: *Geology and petrology of enormous volumes of impact melt on the Moon: a case study of the Orientale basin impact melt sea* (2013)
- <sup>74</sup> Treiman, A.H., Kulis, M.J., Glazner, A.F.: *Spinel-anorthosites on the moon: impact melt origins suggested by enthalpy constraints* (2019)
- <sup>75</sup> Yue, Z., Johnson, B.C., Minton, D.A., Melosh, H.J., Di, K., Hu, W., Liu, Y.: *Projectile remnants in central peaks of lunar impact craters* (2013)
- <sup>76</sup> Longhi, J.: *Experimental petrology and petrogenesis of mare volcanics* (1992)
- <sup>77</sup> Neal, C.R., Taylor, L.A.: *Petrogenesis of mare basalts: A record of lunar volcanism* (1992)
- <sup>78</sup> Shearer, C.K., Papike, J.J.: *Basaltic magmatism on the Moon: a perspective from volcanic picritic glass beads* (1993)
- <sup>79</sup> Shearer, C.K., Papike, J.J.: *Magmatic evolution of the Moon* (1999)
- <sup>80</sup> Hess, P.C., Parmentier, E.M.: *A model for the thermal and chemical evolution of the Moon's interior: Implications for the onset of mare volcanism* (1995)
- <sup>81</sup> Irvine, T.N.: *Origin of chromitite layers in the Muskox Intrusion and other stratiform intrusions: a new interpretation* (1977)
- <sup>82</sup> Irvine, T.N., 1975.: *Olivine-pyroxene-plagioclase relations in the system Mg<sub>2</sub>SiO<sub>4</sub>-CaAl<sub>2</sub>Si<sub>2</sub>O<sub>7</sub>-KAlSi<sub>3</sub>O<sub>8</sub>-SiO<sub>2</sub> and their bearing on the differentiation of stratiform intrusions* (1975)
- <sup>83</sup> Keith, M.L.: *Phase equilibria in the system MgO-Cr<sub>2</sub>O<sub>3</sub>-SiO<sub>2</sub>* (1954)
- <sup>84</sup> Netra S. Pillai, S. Narendranath, K. Vadodariya, Srikar P. Tadepalli et al. *Chandrayaan-2 Large Area Soft X-ray Spectrometer (CLASS): Calibration, In-flight performance and first results*, Icarus, 2021
- <sup>85</sup> Antony Joseph: *Lunar explorations— Discovering water, minerals, and underground caves and tunnel complexes*, 2023
- <sup>86</sup> Chao Zhou: *Chapter 45 Lunar Landscape, Highlands*, Springer Science and Business Media LLC, 2023
- <sup>87</sup> A. Karthi, S. Arivazhagan, Manish Sharma: *Mapping of Compositional Diversity and Chronological Ages of Lunar Farside Multiring Mare Moscoviense Basin: Implications to the Middle Imbrian Mare Basalts*, 2022
- <sup>88</sup> C. M. Pieters: *Mg-spinel lithology: A new rock type on the lunar farside* 2011
- <sup>89</sup> Tianqi Xie, Gordon R. Osinski: *Chapter 189 Shock Metamorphism*" 2023
- <sup>90</sup> Harinthaavimal Balakrishnan: *Polypropylene/organically modified Sabah montmorillonite nanocomposites: Surface modification and nanocomposites characterization* 2011